Insights into post-magmatic metasomatism and Li circulation in granitic systems from phosphate minerals of the Nanping No. 31 pegmatite (SE China)

Can Rao[a,*], Rucheng Wang[b], Yueqing Yang[c], Frédéric Hatert[d], Qunke Xia[a], Xuege Yue[a], Wumengyu Wang[a]

[a] School of Earth Sciences, Zhejiang University, Hangzhou 310027, China

Corresponding author'E-mail: canrao@zju.edu.cn

[b] State Key Laboratory for Mineral Deposits Research, School of Earth Sciences and Engineering, Nanjing University, Nanjing 210046, China

[c] Institute of Mineral resource, Chinese academy of Geological science, Beijing, 100037, China

[d] Laboratoire de Minéralogie, B18, Université de Liège, B–4000 Liège, Belgium

ABSTRACT

Phosphate minerals are key indicators for understanding the processes of diagenesis and mineralization in granitic systems. More importantly, these minerals provide constraints on the post-magmatic behaviour of Li in pegmatite systems that remain to be explored, although Li from early-crystallized Li phosphates is known to leach into hydrothermal fluids. In this study, we performed a detailed petrographic and compositional analysis of phosphate minerals from the Nanping No. 31 pegmatite in southeastern of China, which provides new evidence of Li circulation in granitic systems. Primary phosphate minerals evolved from xenotime and monazite to Mn-rich fluorapatite and then to triphylite and montebrasite, with large amounts of montebrasite in the intermediate zones of the pegmatite, reflecting the increasing activities of both Li and P in peraluminous granitic melts. Montebrasite experienced stages of both high-temperature (360-273℃) and low-temperature (273-100℃) hydrothermal alteration. The high-temperature hydrothermal alteration of montebrasite by Fe- and Mg-rich fluids resulted in the formation of a series of Fe-, Mg-bearing phosphates; the replacement of montebrasite under low-temperature alteration generated amounts of Ca-, Sr-, Ba-bearing phosphate minerals, muscovite and akdalaite $(Al_2O_3)_4 \cdot H_2O$. The formation of micro-networks of akdalaite from montebrasite indicate the low mobility of Al in hydrothermal fluids. A four-stage scenario of post-magmatic Li transport in the Nanping No. 31 pegmatite is proposed: (1) Li derived from the breakdown of primary montebrasite was locally recrystallized and produced secondary montebrasite (Mtb-1); (2) hydrothermal alteration by Fe- and Mg-bearing fluids leached Li from montebrasite to form secondary triphylite and simferite; (3) Li derived from the alteration of montebrasite by Sr-, Ca-rich fluids was involved in the formation of secondary palermoite and bertossaite; and (4) the replacement of secondary triphylite, montebrasite, palermoite and bertossaite by later phases (apatites, ludlamite, anapaite, augelite and fine-grained muscovite) reflect the leaching of Li back into hydrothermal fluids. The re-enrichment of Li during the post-magmatic stage most likely increased the solubility of Ta in the hydrothermal fluids of the granitic pegmatite.

Keywords: phosphate minerals; montebrasite; hydrothermal alteration; akdalaite; Li circulation; Nanping pegmatite.

1. Introduction

Montebrasite, triphylite, apatites and other phosphate phases are common constituents of phosphorus-bearing pegmatites (Moore, 1973; Shigley and Brown 1985). Due to their variable crystallochemical properties and complex paragenesis, these minerals are sensitive to different geochemical conditions in granitic pegmatites (Fransolet, 2007); they thus behave as key indicators of pegmatite differentiation and can be used to better understand the detailed magmatic-hydrothermal processes of pegmatites (Shigley and Brown, 1985). Amblygonite-montebrasite $LiAlPO_4(F,OH)$ and triphylite-lithiophilite $Li(Fe,Mn)PO_4$ group minerals, which are common magmatic Li phases in pegmatites, are often intensively altered to secondary phases during the post-magmatic stages of pegmatite development (e.g., London and Burt, 1982; Fransolet et al., 1986; Baldwin et al., 2000; Roda-Robles et al., 2004; Nizamoff, 2006; Vignola et al., 2008; Hatert et al., 2011; Baijot et al., 2012; Galliski et al., 2012; Shirose and Uehara, 2014). Hydrothermal fluids at the late stage of pegmatite crystallization are also well known to affect spodumene or other Li phases (e.g., London and Burt, 1982; Rao et al., 2012). These metasomatic alterations involve leaching Li from early Li phases into hydrothermal fluids. However, due to the lack of a reliable record of the post-magmatic transport of Li, the circulation of Li in pegmatitic systems is poorly understood. Meanwhile, increasing demand for pegmatitic Li resources (Grosjean et al., 2012; Linnen et al., 2012) and advances in the measurement of Li isotopes (Tomascak et al., 2002; Elliott et al., 2004, 2006; Halama et al., 2009; Pogge von Strandmann and Henderson, 2015; Magna et al., 2016) provide the impetus and mechanisms for understanding the entire Li history of granitic systems.

The Nanping No. 31 pegmatite (Fujian Province, southeastern China) is a highly evolved and mineralized granitic pegmatite (Rao et al., 2009). It is extremely enriched

in Nb, Ta, Sn, Be, and Li and hosts abundant phosphate minerals, thus recording many species and their complex paragenesis. Previous studies of the Nanping No. 31 pegmatite mainly focused on its geology and petrology (Li et al., 1983; Yang et al., 1987), Nb-Ta-Sn-bearing minerals (Yang et al., 1989, 2006; Wang et al., 1999; Rao et al., 2009), and the behaviour of its hydrothermal alterations (Yang et al., 1994, 1995; Rao et al., 2011, 2012, 2014a). Three new mineral species, namely, nanpingite (Yang et al., 1988), strontiohurlbutite (Rao et al., 2014b) and minjiangite (Rao et al., 2015), were first discovered in the Nanping No. 31 pegmatite. In the present study, we investigate the petrologic characteristics and evolution of phosphate minerals and reveal the complex metasomatic processes associated with montebrasite from the Nanping No. 31 pegmatite. Based on these data, we constrain the magmatic and post-magmatic behaviour of Li in the Nanping No. 31 pegmatite. Furthermore, we provide direct evidence of the immobile geochemical behaviour of Al in the hydrothermal fluids, and discuss the influence of Li circulation on the solubilities of Ta in hydrothermal fluids.

2. Geological setting

The Nanping pegmatite zone is located in the northeastern region of the Cathaysia Block in southeastern China (Fig. 1). In this pegmatite zone, the exposed strata can be grouped into the cover and the basement. The cover consists of sedimentary rocks that were deposited between the Late Devonian and the Late Jurassic; the basement is composed of Meso- and Neo-Proterozoic schists and granulites of the Xiafeng fabric in the Wanqun rock suite, which was intruded by most of the Nanping pegmatite dykes (Yang et al., 1987). Folds and faults are well developed in the basement. The Nanping synclinorium is the primary tectonic unit in this field and is further divided into groups of sub-folds with axes oriented to the northeast and from south to north, in which the latter group overlaps the former. The occurrence, shape and distribution of the Nanping pegmatite dykes are mainly controlled by these sub-folds. Different levels of deformation, caused by faults running south to north, northeast, and

northwest, have been found in both the basement and cover rocks. The Hercynian and Yanshanian (Jurassic) granites represent the main magmatic rocks found in this field, both of which are characterized by alkaline, peraluminous rocks with high Si contents and low Ti, Fe, Mg and Ca concentrations (Yang et al., 1987). According to the LA-ICPMS U-Pb dating of columbite-(Fe) and zircon, the emplacement of the Nanping pegmatites occurred at 387 Ma (Tang et al., 2017).

3. Petrographic characteristics of the Nanping pegmatites

The Nanping pegmatite zone includes approximately 500 pegmatite dykes with an outcrop area of approximately 250 km^2. These dykes commonly form lenticular bodies with a general north-northeast strike, are generally 10 to 100 m long (with a maximum length of 600 m) in the direction of strike and are approximately 2 to 10 m wide (with a maximum of 32 m) (see Fig. 2). Based on their different degrees of fractionation, Yang et al. (1987) divided these pegmatites into four groups: muscovite-orthoclase-albite (tabular) pegmatite (type I), muscovite-albite-orthoclase pegmatite (type II), muscovite-orthoclase-albite (fine-grained) pegmatite (type III), and muscovite-albite-spodumene pegmatite (type IV). The type I pegmatite mainly contains 19 vol.% K-feldspar, 35 vol.% albite, 39 vol.% quartz, and 5.9 vol.% muscovite; the type II pegmatite is mainly composed of 27.5 vol.% K-feldspar, 26 vol.% albite, 29.5 vol.% quartz, and 15.5 vol.% muscovite; the type III pegmatite consists of 13 vol.% K-feldspar, 48 vol.% albite, 26 vol.% quartz, 10 vol.% muscovite, and < 5 vol.% spodumene; and the type IV pegmatite is characterized by 4.01 vol.% K-feldspar, 39.98 vol.% albite, 29.95 vol.% quartz, 8.68 vol.% muscovite, 10.92 vol.% spodumene, and 1.02 vol.% montebrasite. From the type I pegmatites to the type IV pegmatites, the Nanping pegmatite varies from the barren to spodumene subtypes. The No. 31 pegmatite is a type IV pegmatite and is one of the most highly evolved and well-mineralized pegmatites in the Nanping pegmatite zone (Yang et al., 1987).

The Nanping No. 31 pegmatite dyke is located at longitude E 118°06', latitude N

26°40', it is a typical LCT-type pegmatite with strong mineralization of Nb, Ta, Sn, Be, and Li (Rao et al., 2009). It is 5 to 6 m in width, 300 to 600 m in length, and extends to a depth of 90 m. The internal textures observed in the quarry 515 m below the surface define five discontinuous mineral-textural zones. From the outermost zone inward (Yang et al., 1987; Rao et al., 2009), they are **Zone I** (the quartz-albite-muscovite zone), which is mainly composed of medium-grained quartz, muscovite and fine-grained albite, with small amounts of accessory minerals such as cassiterite, columbite-tantalite, zircon, beryl, hurlbutite, phenakite, apatite, and strontiohurlbutite; **Zone II** (the saccharoidal albite ± muscovite zone), which is characterized by dominant saccharoidal albite with greenish muscovite and can be further subdivided into subzone IIa (saccharoidal albite > 90 vol%) and subzone IIb (greenish muscovite with 10 vol% quartz and 30 vol% albite), in which Nb-Ta-Sn-bearing oxide minerals such as cassiterite, columbite-tantalite, wodginite, tapiolite-(Fe) are mainly concentrated at the boundary between the two subzones (Rao et al., 2009) and Be-bearing minerals (beryl, phenakite, hydroxyherderite, hurlbutite, euclase and strontiohurlbutite) have also been found (Rao et al., 2011, 2014b); **Zone III** (the albite-quartz-spodumene zone), which is mainly composed of platy crystals of albite, coarse-grained quartz and spodumene, although columbite-tantalite, wodginite-group minerals, tapiolite, microlite, zircon, cassiterite, apatite, montebrasite and beryl are also present in this zone; **Zone IV** (the quartz-spodumene-montebrasite zone), which mainly contains coarse-grained quartz and spodumene and montebrasite crystals, as well as accessory minerals such as columbite-group minerals, wodginite-group minerals, tapiolite-(Fe), microlite, beryl, cassiterite, pollucite, minjiangite, lazulite, kulanite and strontiohurlbutite; and **Zone V** (the blocky quartz-K-feldspar zone) is the pegmatite core and mainly contains blocky quartz and K-feldspar crystals with a small amount of accessory minerals.

4. Analytical methods

In this study, a suite of rock samples was collected from the mine quarry excavated

515 m below the surface in the Nanping No. 31 pegmatite dyke. A total of 31 phosphate mineral species were identified based on their petrologic and chemical features (Table 1). The chemical compositions of these minerals were obtained by using a JEOL JXA-8100M electron microprobe to perform wavelength-dispersion spectrometry (WDS mode, with settings of 15 kV, 20 nA, and a beam diameter of 1 μm). Measurements were performed in the State Key Laboratory for Mineral Deposits Research at Nanjing University. Element peaks and backgrounds were measured with counting times of 10 s and 5 s, respectively. The following standards were used: albite (Si), hornblende (Na, K, Mg, Al, Ca, and Fe), fluorapatite (P and F), $MnTiO_4$ (Mn and Ti), synthetic $Ba_3(PO_4)_2$ (Ba), and synthetic $SrSO_4$ (Sr). A computer program that implements the ZAF method was used for all data reduction. The contents of Li_2O, BeO and H_2O in phosphate minerals were estimated by stoichiometry.

Powder XRD patterns were collected from finely ground samples spread on glass slides using a RIGAKU D/max Rapid IIR micro-diffractometer (CuKα, λ = 1.54056 Å). These measurements were performed in the School of Earth Sciences and Info-physics at Central South University in China. The micro-diffractometer was operated with a Gandolfi-like motion, under conditions of 48 kV and 25 mA, using a 0.05 mm diameter collimator; the total exposure time was 2 hr. Structural models of fluorapatite and akdalaite (see below) were used to refine the powder XRD data.

5. Mineralogy of phosphate minerals

5.1. Montebrasite $LiAl(PO_4)(OH,F)$

Montebrasite occurs as one of the main rock-forming minerals in the Nanping No. 31 pegmatite. According to petrographic relationships, montebrasite occurs as both primary and secondary phases in different zones of this pegmatite. Primary montebrasite is distributed with variable abundance and different occurrences in zones I, III and IV (Table 1). In zone I, montebrasite occurs as discrete crystals up to one millimeter long between quartz and fine-grained albite; some crystals are replaced by late fine-grained muscovite and fluorapatite (Fig. 3a). Montebrasite from zone III

forms anhedral crystals up to 10 cm long, and is interstitial to coarse albite or located between quartz and spodumene. In some cases, montebrasite crystals have been progressively altered to lazulite, palermoite and fluorapatite (Fig. 3b). Massive montebrasite crystals mainly appear in zone IV; they are generally 20 to 40 cm long and are closely associated with massive quartz, spodumene, beryl, Nb-Ta-bearing oxides, cassiterite, and muscovite. Chemically, primary montebrasite has low F contents, which decrease from the outer zones of the pegmatite moving inward (the average F content in montebrasite is 1.59 wt.% in zone I and 1.27 wt.% in zone IV, Table 2).

Secondary montebrasite mainly occurs in zones III and IV, in which three different types of secondary montebrasite were distinguished based on their petrological features and paragenetic relationships. The most common occurrence is represented by secondary montebrasite (Mtb-1), which forms small crystals, up to 500 μm in diameter, along the fractures or rims of massive montebrasite in zones III and IV (e.g. Fig. 4a). The second occurrence is characterized by montebrasite assemblages (Mtb-2) that are up to 400 μm in diameter and form along the cleavage planes and/or rims of lazulite crystals in zone IV (Fig. 4b). In some cases, this type of secondary montebrasite occurs in the cleavage planes of lazulite, forming up to 40 μm long veinlets (Fig. 4c). Irregular assemblages or veinlets of montebrasite (Mtb-3) were observed in the fractures and rims associated with palermoite or bertossaite in zone IV (Fig. 4d). The results of electron microprobe analyses indicate that the chemical compositions of secondary montebrasite are similar, as they contain very low F contents (with an average value of 0.10 wt.% F), which are indicative of almost end-member montebrasite (Table 2).

5.2. Apatites $Ca_5(PO_4)_3(F,OH)$

Apatite group minerals occur as primary and secondary phases in different zones of the Nanping No. 31 pegmatite. Primary apatites are more abundant, but secondary apatites are more mineralogically diverse. Primary apatites generally form light green euhedral to subhedral or granular crystals up to 20 centimeters long; the sizes of the apatite crystals increase from the outer zones inward. Secondary apatites generally

occur as the alteration products of primary and/or early phosphate minerals and were deposited during the different hydrothermal stages of the Nanping No. 31 pegmatite (Fig. 3 and Fig. 4). They generally form irregular aggregates and/or veinlets, which are intergrown with secondary quartz and fine-grained muscovite among the alteration assemblages of montebrasite. In some cases, Sr-rich apatites replace early apatites, forming veinlets, rims or mosaic-like phases in the hydrothermal alteration mineral assemblages formed from montebrasite. Electron microprobe analyses show that primary apatites are enriched in F and Mn (up to 4.79 wt.% F and 5.42 wt.% MnO, respectively), which correspond to Mn-rich fluorapatite (Table 3 and Fig. 5). In contrast, secondary apatites are enriched in Sr (with an average value of 1.67 wt.% SrO, but ranging up to 12.8 wt.% SrO) and are classified as hydroxy-fluorapatite (Table 3). The variation of SrO and MnO/FeO in secondary apatites is shown in Figure 5.

5.3. Triphylite $LiFe(PO_4)$

Both primary and secondary triphylite have been found in the Nanping No. 31 pegmatite (Rao et al., 2014a). Primary triphylite forms small granular aggregates approximately 80 to 200 μm in diameter in the rocks of zones III and IV and is associated with lazulite, wagnerite, fluorarrojadite-(BaNa), palermoite, and fluorapatite. Secondary triphylite occurs as veinlets or aggregates along the fractures and rims of primary montebrasite (Fig. 4a and Fig. 6a) and quartz (Fig. 6b) in zone IV. Triphylite veinlets are up to 1 mm wide and several cm long. They are associated with fine-grained muscovite, fluorapatite, ludlamite, anapaite, wagnerite and fluorarrojadite-(BaNa). Some Nb-Ta-bearing oxide (tantalite) crystals are observed in the triphylite assemblage (Fig. 6a). The chemical features of triphylite have been described in our previous study (Rao et al., 2014a).

5.4. Wagnerite $Mg_2(PO_4)F$

Wagnerite occurs in two different modes in the Nanping No. 31 pegmatite. It occurs as one of the hydrothermal alteration products (denoted wag-1) of triphylite (Fig. 6b, and Fig. 5a: Rao et al., 2014a) and as anhedral crystals (denoted wag-2) along fractures developed in montebrasite in zone IV (Fig. 6c). The representative

compositions of wagnerite are given in Table 4. Compared to the anhedral crystals of wagnerite (wag-2), which contain, on average, 7.77 wt.% F, 5.61 wt.% FeO, 0.79 wt.% MnO and 45.29 wt.% MgO, irregular assemblages of wagnerite (wag-1) have clearly higher concentrations of F, Mn and Fe (with average values of 11.08 wt.% F, 4.20 wt.% MnO and 11.24 wt.% FeO) but lower concentrations of Mg (with an average of 37.74 wt.% MgO).

5.5. Lazulite $MgAl_2(PO_4)_2(OH)_2$

In hand specimens, lazulite appears as blue granular aggregates along the fractures of primary montebrasite. Based on their petrological textures and chemical compositions, three different types of lazulite were distinguished. The first type of lazulite (denoted laz-1) is characterized by subhedral to euhedral crystals up to 150 μm long, which are included in the secondary montebrasite assemblage from zone IV (Fig. 4b). They are closely associated with palermoite, bertossaite, augelite, fluorapatite and fluorarrojadite-(BaNa). In back-scattered electron (BSE) images, they are weakly heterogeneous, consisting of intergrown brighter and darker areas; the brighter areas are slightly enriched in Fe compared to the darker areas. The second type of lazulite (denoted laz-2) occurs as anhedral grains, irregular assemblages around primary montebrasite crystals (Figs 3b, 4c and 6d), or along fractures in the central portions of granular aggregates of triphylite (Fig. 5a: Rao et al., 2014a). Wagnerite, fluorarrojadite-(BaNa), fluorapatite, palermoite and bertossaite were also observed in these assemblages. Lazulite veinlets (denoted laz-3) represent the third type of lazulite, which occurs along cleavage faces or fractures in montebrasite in zone IV (Fig. 6e). These veinlets are approximately 1 μm wide but up to hundreds of μm long and are rimmed by fine-grained muscovite and palermoite.

The results of electron microprobe analyses indicate that the P content of lazulites is slightly less than the ideal value, but their Al content is close to or slightly higher than the ideal value (Table 4). Lazulite-1 has relatively high Fe concentrations but low Mg concentrations, with contents of approximately 11.09 wt. % FeO and 6.9 wt. % MgO, which are indicative of Fe-rich lazulite; the chemical compositions of lazulite-2 and lazulite-3 are similar (Table 4). The MgO contents of these lazulites range from

9.10 to 11.77 wt. % (with an average value of 10.96 wt. %). Their FeO contents range from 2.30 to 6.81 wt. % (with an average value of 4.04 wt. %), with minor concentration of K, Na, Mn, Ti, Sr, Ba, Si, and Ca but no F.

5.6. Palermoite-bertossaite $SrLi_2Al_4(PO_4)_4(OH)_4$ - $CaLi_2Al_4(PO_4)_4(OH)_4$

Palermoite and bertossaite are end-members of a Sr-Ca isomorphic series with an ideal chemical formula of $Li_2(Sr,Ca)Al_4(PO_4)_4(OH)_4$, which occur as secondary phases of montebrasite in zones III and IV of the Nanping No. 31 pegmatite. Palermoite commonly forms fine grains or nodules up to 600 μm wide, and is distributed among fine-grained muscovite. Lazulite, secondary montebrasite, kulanite, minjiangite, goyazite and fluorapatite are also observed in these assemblages. In some cases, irregular assemblages, approximately 1 to 2 cm in diameter, are observed around montebrasite crystals in zone IV; additionally, palermoite veinlets are located in the rims of primary montebrasite in zone III (Fig. 3b) or as intergrowths with fine-grained muscovite in the fractures developed in primary montebrasite in zone IV (Fig. 6e and Fig. 7b)

Bertossaite formed slightly later than palermoite in the Nanping No. 31 pegmatite. It generally occurs as irregular assemblages around palermoite (Fig. 7a) or forms veinlets crosscutting montebrasite (Fig. 7c). Its associated minerals include kulanite, goyazite, hydroxylapatite, and fine-grained muscovite. Bertossaite is also observed as irregular assemblages up to 2 cm in diameter or intergrown with secondary montebrasite (mtb-3) among the alteration products of primary montebrasite in zone IV (Fig. 4d). In some cases, bertossaite crystals were observed to be altered to augelite (Fig. 7d). Electron microprobe analyses results indicate that palermoite and bertossaite are members of a continuous isomorphous series of (Sr, Ca); they contain 0.19 to 13.10 wt% SrO and 0.83 to 8.89 wt% CaO (Table 4).

5.7. Kulanite $BaFe^{2+}_2Al_2(PO_4)_3(OH)_3$

Kulanite generally occurs as small grains distributed among the hydrothermal alteration products of massive montebrasite in zone IV. It occurs along the fractures developed in lazulite, or forms veinlets up to 1 centimeter long within the assemblage of bertossaite + montebrasite (Fig. 7c). Fluorapatite, goyazite, secondary montebrasite,

palermoite, and fine-grained muscovite are found in this assemblage. Chemically, kulanite contains 15.70 to 16.99 wt.% Al_2O_3, 33.62 to 35.41 wt.% P_2O_5, 22.01 to 25.52 wt.% BaO, 6.59 to 12.95 wt.% FeO, 5.20 to 12.78 wt.% MnO, 0.27 to 3.01 wt.% MgO, < 2.50 wt.% SrO, < 1.72 wt.% TiO_2, and minor K_2O, Na_2O, CaO, SiO_2 and F (Table 4).

5.8. Simferite $Li(Mg,Fe^{3+},Mn^{3+})_2(PO_4)_2$

Simferite occurs as small orange grains or irregular assemblages along the rims of primary montebrasite crystals in zone IV (Fig. 6f). The sizes of the simferite grains range from 50 to 100 μm in diameter. Its associated minerals contain secondary montebrasite, fluorapatite, ludlamite and fine-grained muscovite. The results of electron microprobe microprobe analyses indicate that simferite contains average values of 50.86 wt.% P_2O_5, 18.66 wt.% MgO, 14.72 wt.% FeO (16.34 wt.% Fe_2O_3), and 5.38 wt.% MnO (5.97 wt.% Mn_2O_3), as well as minor amounts of K_2O, Na_2O, CaO, SrO, BaO, SiO_2, and F (< 1 wt.% in total).

5.9. Accessory phosphates

Goyazite $SrAl_3(PO_4)_2(OH)_5{\cdot}(H_2O)$ is a relatively late secondary phosphate phase in the Nanping No. 31 pegmatite. It occurs as veinlets up to hundreds of μm long that fill the interstices between albite crystals in zone II, as well as fractures developed in bertossaite in zone IV. Its associated minerals are hydroxylapatite, kulanite, palermoite, secondary montebrasite and fine grained muscovite. Goyazite contains 13.92 to 20.19 wt.% SrO and up to 3.51 wt.% BaO (Table 4).

Augelite $Al_2(PO_4)(OH)_3$ occurs as one of the hydrothermal alteration products of montebrasite in the Nanping No. 31 pegmatite. It forms euhedral to subhedral crystals, and occurs, together with secondary montebrasite, palermoite, and fluorapatite, around primary montebrasite in zone IV. However, augelite also occurs as one of the alteration products of bertossaite in zone IV (Fig. 7d); some remnants of bertossaite are sporadically distributed in the augelite assemblages. Chemically, augelite contains approximately 36 wt. % P_2O_5 and 50 wt. % Al_2O_3, with low concentrations of minor elements (total < 1 wt. %), suggesting that it is an end-member phase.

Beryllonite $NaBePO_4$ was detected by microprobe analysis in one thin section from zone I. It forms anhedral crystals up to 30 μm long between quartz and muscovite, and is associated with strontiohurlbutite, hydroxylapatite, and hydroxylherderite. Chemically, beryllonite contains 57.06 wt.% P_2O_5 and 20.11 wt.% Na_2O, as well as small amounts of K_2O, FeO, MnO, MgO, CaO, SrO, BaO, and SiO_2 (< 1 wt.% in total).

Phosphoferrite occurs as irregular assemblages among the alteration products of montebrasite. Its chemical composition data indicate that phosphoferrite has an empirical formula corresponding to $(Fe^{2+}_{2.74},Mn_{0.26}, Mg_{0.03})_{\Sigma 3.03}(PO_4)_2 \cdot 3(H_2O)$.

6. Alteration assemblages of montebrasite

Both primary montebrasite and secondary montebrasite (Mtb-1) in the Nanping No. 31 pegmatite were strongly affected by late hydrothermal fluids, which produced different secondary phases. Here, five distinct types of alteration assemblages of montebrasite were distinguished and are described below.

Triphylite ± wagnerite + fluorapatite assemblage. This alteration assemblage of montebrasite mainly consists of triphylite, wagnerite and fluorapatite in zone IV. This type of triphylite is restricted to primary montebrasite; it occurs as fine-grained crystals along fractures within montebrasite. Wagnerite typically surrounds crystals of triphylite (Fig. 6b). In some cases, montebrasite has been replaced by wagnerite (Fig. 6c). Fluorapatite, muscovite and fluorarrojadite are also observed in this assemblage.

Lazulite + palermoite + fluorapatite assemblage. Lazulite is one of the most common alteration products of montebrasite in the Nanping No. 31 pegmatite. It generally occurs as irregular aggregates (Fig. 6d) or veinlets (Fig. 6e) along the rims or fractures of montebrasite. Palermoite formed later than lazulite; it occurs as veinlets surrounding the aggregates of lazulite + montebrasite in zone III (Fig. 3b), or the rims of the alteration products of montebrasite in zone IV (Fig. 6e), or as irregular aggregates crosscutting the early alteration products of montebrasite (Fig. 6d). In this

assemblage, fluorapatite is the youngest phase, as it crosscuts both lazulite and palermoite.

Palermoite + bertossaite + kulanite + fluorapatite assemblage. In the Nanping No. 31 pegmatite, both palermoite and bertossaite occur as alteration products of montebrasite along the rims and fractures of primary montebrasite (Fig. 4d, Fig. 7a and Fig. 7c). Palermoite veinlets are commonly observed among the alteration products of montebrasite (Fig. 3b, Fig. 6e and Fig. 7b). In addition, palermoite is generally replaced by bertossaite along its rims and fractures (Fig. 7a and Fig. 7d). Kulanite, fluorapatite, goyazite and minjiangite also occur in this assemblage.

Simferite + fluorapatite assemblage. In addition to triphylite, palermoite and bertossaite, simferite is another secondary Li phosphate formed from montebrasite. It occurs as small orange grains among the fine-grained muscovite formed from the primary montebrasite in zone IV (Fig. 6f). Fluorapatite generally surrounds the orange grains or occurs as irregular aggregates in this assemblage.

Fluorapatite + akdalaite assemblage. Apatites are common phases produced by the hydrothermal alteration of montebrasite. They commonly occur as veinlets crosscutting earlier phases, or as irregular aggregates along the rims and fractures of the alteration products of montebrasite. In zone IV, some montebrasite crystals are notably rimmed by veinlets that are approximately 50 to 200 μm wide (Fig. 8a and Fig. 8b). Under crossed polarizers, they are isotropically black (Fig. 8a). The results of electron microprobe analyses indicate that these veinlets are mainly composed of CaO, Al_2O_3, P_2O_5 and F. However, scanning electron microscope (SEM) analyses indicate that they are composed of brighter and darker regions, which form micron-scale networks (Fig. 8c and Fig. 8d). The powder X-ray diffraction patterns observed by in-situ micro-diffraction analyses was shown in Figure 9, which appear to display two differently indexed X-ray diffraction patterns. The brighter phase, which has six distinct lines [*d* in Å(*I*)(*hkl*)]: 2.803(100)(211), 2.776(81)(112), 2.706(29)(300), 1.936(34)(222), 1.837 (39)(213) and 1.797(14)(321), corresponds to fluorapatite with $\boldsymbol{a}$ =9.370 (2) Å, $\boldsymbol{c}$ = 6.877 (2) Å, and $\boldsymbol{V}$ = 522.9 Å^3. The darker phase has eight distinct lines [*d* in Å(*I*)(*hkl*)]: 2.502(34)(006), 2.317(52)(412), 2.114(94)(324), 1.862(20)(334),

1.681(24)(523), 1.418(100)(445), 1.394(56)(329) and 1.215(51)(20 12) and unit cell parameters of $\boldsymbol{a}$ = 12.889(9) Å, $\boldsymbol{c}$ = 14.949(7) Å, and $\boldsymbol{V}$ = 2150.83 Å^3, which is indicative of akdalaite, $(Al_2O_3)_4 \cdot H_2O$. These patterns and peak data are in agreement with those of fluorapatite from ICDD pdf No. 15-0876 and akdalaite from ICDD pdf No. 25-0017, respectively.

7. Discussion

7.1. Genetic sequence of primary phosphates

Phosphate minerals are common accessory phases in granitic bodies such as the Beauvoir granite of France (Charoy, 1999), the Tanco pegmatite of Canada (Černá et al., 1972), the Cañada pegmatite of Spain (Roda-Robles et al., 2004), and the Palermo #2 pegmatite in the U.S.A. (Nizamoff, 2006). Montebrasite-amblygonite and lithiophilite-triphylite commonly occur as subhedral crystals or rounded nodules embedded in rock-forming minerals within different zones in pegmatites (e.g., London and Burt, 1982; Galliski et al., 2012). The magmatic crystallization and evolution of these phosphates are believed to be controlled by their solubilities and the incompatible behaviour of P in granitic melts (Roda-Robles et al., 2004; Roda-Robles et al., 2012). The low solubilities of phosphates in granitic melts could result in their crystallization, while the incompatible behaviour of P can enhance the evolution of phosphates and cause the abundance of phosphates to increase.

Table 1 shows the distribution and crystallization sequence of primary phosphate minerals in the Nanping No. 31 pegmatite. REE-bearing phosphates (xenotime and monazite) occur in the border zone (zone I) of the pegmatite (Yang et al., 1987), indicating that they were formed by early magmatic crystallization. This geochemical trend can be attributed to the low solubilities of xenotime and monazite in peraluminous granitic melts (Montel, 1986; Wolf and London, 1995). Similar occurrences of xenotime and monazite have been found in the Palermo #2 pegmatite in New Hampshire, U.S.A. (Nizamoff, 2006). Primary fluorapatite, which occurs as euhedral to subhedral or granular crystals, is associated with rock-forming minerals

436 such as quartz, albite and muscovite in different zones and is enriched in Mn and F
437 (Table 3 and Fig. 5), suggesting that it was formed by early magmatic crystallization.
438 This feature is in agreement with previous studies of fluorapatite from the Silbergrube
439 Aplite (SA) of the Hagendorf-Pleystein pegmatite district (Dill et al., 2008).
440 Roda-Robles et al. (2004) suggested that Mn-rich fluorapatite is formed after the
441 crystallization of xenotime. The crystallization of triphylite and montebrasite, as well
442 as spodumene, which mainly occur in zones III and IV, represents the magmatic Li
443 stage of the Nanping No. 31 pegmatite. London and Burt (1982) suggested that
444 primary Li phosphates appear to crystallize after spodumene. Triphylite generally
445 crystallizes shortly before the magmatic Li stage (Ginsburg, 1960). In the Nanping No.
446 31 pegmatite, small montebrasite crystals occur in the out zone (zone I) of the
447 pegmatite (Fig. 3a), whereas spodumene and triphylite are only found in the
448 intermediate pegmatite zones (zones III and IV) (Rao et al., 2012, 2014a). Therefore,
449 spodumene and triphylite likely began to crystallize somewhat later, but finished
450 crystallizing before the formation of montebrasite. Montebrasite crystals are massive
451 and abundant in the exocontact zone of the pegmatite core (zone IV), thus reflecting
452 the incompatible behaviour of P in granitic melts. The observed decrease in F content
453 in primary montebrasite from the outer zones inward (Table 2) is consistent with
454 magmatic differentiation.
455
456 ***7.2. Hydrothermal alteration of montebrasite***
457 In granitic pegmatites, montebrasite is generally affected by post-magmatic fluids,
458 which can initiate various metasomatic and/or dissolution-crystallization processes
459 and generate different sequences of metasomatic alterations (e.g., London and Burt,
460 1982; Baldwin et al., 2000; Galliski et al., 2012; Shirose and Uehara, 2014).
461 Montebrasite from the White Picacho pegmatites was gradually replaced by low-F
462 montebrasite, hydroxylapatite + crandallite, then by hydroxylapatite + muscovite +
463 brazilianite + augelite + scorzalite + kulanite + wyllieite, and finally by muscovite and
464 carbonate + apatites (London and Burt, 1982). Baldwin et al. (2000) suggested that
465 natromontebrasite, brazilianite, lazulite, scorzalite, goyazite, gorceixite, crandallite,

hydroxylapatite and muscovite are the typical alteration products of montebrasite. Nizamoff (2006) further divided montebrasite alteration into high- and low-temperature stages of metasomatic alteration, which occur under both oxidizing and non-oxidizing conditions. In the Nanping No. 31 pegmatite, the textural relationships of alteration assemblages (Fig. 3, Fig. 4, Fig. 6, Fig. 7 and Fig. 8) indicate that multiple periods of hydrothermal alteration of montebrasite occurred. Yang et al. (1987, 1994) suggested that the emplacement temperature of the Nanping No. 31 pegmatite is 420-360℃, with the end magmatic crystallization temperature (273 ℃). Therefore, the metasomatic alteration of montebrasite can be split into high-temperature (360 to 273 ℃) and low-temperature (273-100 ℃) alteration stages (Fig. 10).

During the high-temperature alteration stage, the transformation of montebrasite to low-F montebrasite could have been the first alteration process of primary montebrasite to occur (London and Burt, 1982; Baldwin et al., 2000). This process is attributed to the exchange of OH for F and occurs after the completion of magmatic crystallization due to the increasing α_{H2O} in post-magmatic fluids (Galliski et al., 2012). Then, Li-leaching and/or Fe^{2+}/Mg^{2+} cation exchange processes, caused by Fe- and Mg-rich fluids, generate Fe/Mg phosphate minerals such as lazulite, wagnerite, triphylite, and simferite (Fig. 10), which suggests that early-stage hydrothermal fluids have relatively high activities of Mg and F. This feature is in good agreement with previous studies of fluid inclusions in the Nanping pegmatite (Yang et al., 1994). The alteration of montebrasite to lazulite and wagnerite involves Li leaching and Fe^{2+}/Mg^{2+} cation exchanges. The Fe^{2+}/Mg^{2+}-rich hydrothermal fluids were possibly derived from the hydrothermal alteration of pre-existing pegmatite minerals such as primary triphylite (Rao et al., 2014a) The presence of triphylite veinlets in fractures developed within primary montebrasite (Fig. 4a and (Fig. 6a), and the occurrence of simferite aggregates around primary montebrasite (Fig. 6f), reflect the dissolution of montebrasite and reprecipitation of Li phases from hydrothermal fluids. The occurrence of simferite, which is a typical Fe^{3+}-bearing phase, suggests that it occurred under oxidizing conditions. The crystallization sequence of triphylite,

wagnerite and simferite suggests that the hydrothermal fluids were transformed from non-oxidizing to oxidizing conditions. These Mg-/Fe-bearing phases, however, were also affected by later hydrothermal fluids such as Ca-rich fluids, resulting in the crystallization of ludlamite, phosphoferrite and anapaite.

Both primary montebrasite and secondary montebrasite (Mtb-1) during the low-temperature alteration stage were subsequently affected by different Ca-, Sr-, and Ba-rich hydrothermal fluids. These processes likely reflect Ca-, Sr-, and Ba-cation exchanges and the K+H processes of montebrasite, which are responsible for the formation of the diverse suite of secondary phosphates (Fig. 10). Apatites are the most common and main phases among the hydrothermal alteration products of montebrasite, indicating that Ca is dominant within hydrothermal fluids. The presence of palermoite (Fig. 3b, Fig. 6e and Fig. 7b), strontiohurlbutite and goyazite, as well as secondary Sr-rich apatites, reflect the replacement of montebrasite by different Sr-rich fluids. Goyazite commonly crystallized as veinlets slightly later than palermoite and strontiohurlbutite. The crystallization of bertossaite after palermoite (Fig. 7a and Fig. 7d), indicates that another exchange of Ca for Sr occurred in late hydrothermal fluids. Minjiangite and fluorarrojadite-(BaNa) generally formed after the palermoite group minerals in montebrasite alteration assemblages, reflecting replacements from Ba-rich fluids that occurred after replacements from Sr-rich fluids. The presence of muscovite as fine-grained assemblages or veinlets among alteration assemblages of montebrasite corresponds to the K+H processes of montebrasite. Shirose and Uehara (2014) suggested that this type of muscovite crystallized in acidic hydrothermal fluids associated with pegmatites. Akdalaite was first observed as one of alteration products of montebrasite. The micron-scale network structures (Fig. 8) reflect a typical process of dissolution and re-precipitation (Putnis and Austrheim, 2010).

7.3. Li circulation in the Nanping No. 31 pegmatite

In Li-bearing pegmatites, spodumene, montebrasite and triphylite group minerals are the main carriers of Li (Charoy et al., 2001). Due to their instability in hydrothermal fluids, these Li minerals are extensively altered in pegmatites (e.g.,

London and Burt, 1982). The exchange of Na for Li in spodumene is considered to represent the albitization of pegmatite (London and Burt, 1982; Charoy et al., 2001). The Quensel-Mason sequence in triphylite group minerals involves the progressive oxidation of Fe and Mn (Fransolet, 2007). These processes result in the leaching of Li into hydrothermal fluids associated with pegmatites. London and Burt (1982) suggested that some of the Li leached from the hydrothermal alteration of primary Li-bearing minerals is subsequently incorporated into the fine-grained muscovite and tourmaline at the exocontacts of pegmatites. In the Nanping No. 31 pegmatite, the extreme Li enrichment of the magma induced the successive crystallization of spodumene, triphylite and montebrasite. Spodumene and triphylite were strongly affected by post-magmatic fluids (Rao et al., 2012, 2014a), but no secondary Li phases were found; only late tourmaline contains up to 0.49 wt.% Li_2O (Rao et al., 2012). Various secondary Li phases formed by the hydrothermal alteration of montebrasite (Fig. 10), however, reflect the dissolution, transport and crystallization of Li in the post-magmatic stages of the Nanping No. 31 pegmatite.

The occurrence and crystallization sequence of secondary Li phases suggest that four Li circulations occurred in the Nanping No. 31 pegmatite. The transformation of primary montebrasite to secondary montebrasite (Mtb-1) (Fig. 4a) could have been the first stage of circulation of Li in the pegmatite. This process reflects the dissolution and local recrystallization of Li-bearing minerals. During the high-temperature alteration stage, primary montebrasite and secondary montebrasite (Mtb-1) were replaced by lazulite, wagnerite, augelite and fluorapatite (Fig. 10), resulting in the leaching of Li into hydrothermal fluids. These Li-rich fluids, however, were likely responsible for the formation of secondary Li phases such as triphylite (Fig. 4a) and simferite (Fig. 6f). Therefore, the dissolution of Li minerals by Fe-/Mg-rich fluids, transport of Li and the crystallization of secondary Li minerals, comprise the second stage of Li circulation. The presence of secondary montebrasite (Mtb-2 and Mtb-3) (Fig. 4b-d), palermoite veinlets (Fig. 3b, Fig. 6e and Fig. 8b) and bertossaite veinlets (Fig. 7a and Fig. 7c) suggest a relatively late stage of Li circulation in hydrothermal fluids. The replacement of bertossaite by augelite (Fig.

7d), and the replacement of secondary triphylite by late phases reflect the leaching of Li from secondary Li minerals into the hydrothermal fluids. It must be noted that, however, compared to the Li released from the primary Li minerals, large amounts of Li were leached from the pegmatite by the hydrothermal fluids so far as to be carried out of the pegmatite, only small amounts of Li were preserved in secondary Li-bearing minerals.

In the Nanping No. 31 pegmatite, it must be noted that Nb-, Ta-, Sn- and Be-bearing minerals increase with abundances from outer zones inward in parallel with the enrichment of Li (Rao et al., 2009). These rare-metal-bearing minerals were traditionally considered as magmatic phases in pegmatites such as the Tanco pegmatite of Canada (Černá et al., 1972) and the Palermo #2 pegmatite in the U.S.A. (Nizamoff, 2006). However, small tantalite crystals occur in the secondary triphylite formed from primary montebrasite (Fig. 6a). This textural relationship suggests that the crystallization of tantalite is related to the high-temperature alteration of montebrasite by Fe-/Mg-rich hydrothermal fluids. Indeed, a network of veinlets of secondary tantalite has been observed in the Nanping No. 31 pegmatite (Rao et al., 2009), which is suggestive of the existence of Ta-rich fluids. In this case, the associated spodumene was also strongly affected by late hydrothermal fluids, resulting in the leaching of Li into the hydrothermal fluids. This implies that the replacement of Li phases during the process of metasomatic alteration promotes the enrichment of Ta in hydrothermal fluids but that the Ta crystallized before secondary Li phases. Therefore, the enrichment of Li during the hydrothermal stages of the pegmatite could possibly increase the solubility of Ta in hydrothermal fluids (Zaraisky et al., 2010) .

7.4. Transport of Al in the hydrothermal fluids

Aluminium generally behaves as an immobile element under hydrothermal conditions (Carmichael, 1969; Salvi et al., 1998). During metasomatic processes, therefore, Al is transferred from one phase to other phases (Kister et al., 2006). In the Nanping No. 31 pegmatite, the hydrothermal alteration of montebrasite resulted in the

586 formation of various Al-bearing phosphate minerals, such as palermoite, bertossaite,
587 lazulite, kulanite, goyazite, crandallite, augelite and fluorarrojadite, indicating the
588 local transformation of Al-bearing phases by hydrothermal fluids. Although non-Al
589 phosphate phases, such as apatites, triphylite, wagnerite, and anapaite, are present in
590 the alteration assemblages, they are associated with fine-grained muscovite (Fig. 3a,
591 Fig. 6a, Fig. 6b and Fig. 6e). These features indicate that Al cannot be transported
592 long distances by late-stage hydrothermal fluids.

593 Akdalaite $(Al_2O_3)_4 \cdot H_2O$ was first reported by Shpanovet et al. (1970); it occurs as
594 veinlets cutting through amesite-fluorite-muscovite rock and fluorite-magnetite-
595 diopside-vesuvianite skarn from Kazakhstan. After this initial description, no natural
596 akdalaite was reported. In the Nanping No. 31 pegmatite, however, akdalaite and
597 fluorapatite form micro-network phases as the alteration products of montebrasite (Fig.
598 8). This textural relationship supports the immobile geochemical behaviour of Al in
599 the hydrothermal fluids. In fact, corundum produced by spodumene alteration has also
600 been observed in the Nanping No. 31 pegmatite (Rao et al., 2012).
601

602 ## 8. Conclusions

603 (1) Primary phosphate minerals from the Nanping No. 31 pegmatite evolved from
604 xenotime and monazite to Mn-rich fluorapatite and then to triphylite and
605 montebrasite, reflecting the increasing activities of both Li and P in peraluminous
606 granitic melts. The formation of secondary phosphate minerals is mainly related
607 to the metasomatic alteration of montebrasite.

608 (2) Montebrasite experienced high-temperature (360 to 273 ℃) and low-temperature
609 (273-100 ℃) hydrothermal alteration stages. The high-temperature hydrothermal
610 alteration of montebrasite mainly corresponds to Li-leaching and/or $(Fe,Mg)^{2+}$
611 cation exchange processes, which produced a series of Fe-/Mg-bearing
612 phosphates. The low-temperature hydrothermal alteration of primary
613 montebrasite and secondary montebrasite (Mtb-1) is related to Ca-, Sr-, and
614 Ba-cation exchanges and K + H processes in the hydrothermal fluids, resulting in

615 the formation of Ca-, Sr-, Ba-bearing phosphate minerals, muscovite and
616 akdalaite. The hydrothermal fluids underwent a transformation from
617 non-oxidizing conditions to oxidizing conditions.
618 (3) Montebrasite, triphylite and spodumene, which are the magmatic carriers of Li in
619 the Nanping No. 31 pegmatite, were strongly affected by late hydrothermal fluids.
620 Four stages of the post-magmatic circulation of Li were proposed: first, secondary
621 montebrasite (Mtb-1) reflects the local circulation of Li; then, Li derived from the
622 high-temperature hydrothermal alteration of montebrasite by Fe-Mg-bearing
623 fluids is combined with Fe and Mg to form secondary Li-bearing phases such as
624 triphylite and simferite; then, Li derived from the low-temperature hydrothermal
625 alteration of montebrasite by Sr-Ca-rich fluids is involved in the formation of
626 secondary palermoite, bertossaite and montebrasite (Mtb-2 and Mtb-3); finally,
627 the replacement of secondary triphylite, montebrasite, palermoite and bertossaite
628 by later phases results in the leaching of Li back into hydrothermal fluids. The
629 re-enrichment of Li during the hydrothermal stages could have increased the
630 solubility of Ta in the hydrothermal fluids derived from the granitic pegmatite.
631 (4) Al derived from the hydrothermal alteration of montebrasite was combined with
632 other ions into secondary Al minerals such as lazulite, palermoite, bertossaite,
633 goyazite, and muscovite. The micro-networks of akdalaite $(Al_2O_3)_4 \cdot H_2O$, which
634 were first found as one of the secondary phases of montebrasite, clearly
635 demonstrate the low mobility of Al in hydrothermal fluids.
636
637 **Acknowledgements** This paper benefitted from critical comments of H.G. Dill, P.
638 Tomascak, and Editor F. Pirajno. Their careful comments and helpful suggestions
639 improved greatly our manuscript. Financial support for the research was provided by
640 NSF of China (Grant No. 41472036) and the Fundamental Research Funds for the
641 Central Universities.
642

References

Baijot, M., Hatert, F., Philippo, S., 2012. Mineralogy and geochemistry of phosphates and silicates in the Sapucaia pegmatite, Minas Gerais, Brazil: genetic implications. Can. Mineral. 50, 1531–1554.

Baldwin, J.R., Hill, P.G., Von Knorring, O., Oliver, G.J.H., 2000. Exotic aluminum phosphates, natromon-tebrasite, brazilianite, goyazite, gorceixite and crandallite from rare-element pegmatites in Namibia. Mineral .Mag. 64, 1147–1164.

Carmichael, D.M., 1969. On the mechanism of prograde metamorphic reactions in quartz-bearing pelitic rocks. Contrib. Mineral. Petrol. 20, 244–267.

Černá, I., Černý, P., Ferguson, R.B., 1972. The Tanco pegmatite at Bernic Lake, Manitoba; III, Amblygonite-montebrasite. Can. Mineral. 11, 643–659.

Černý, P., Ercit, T.S., 2005. The classification of granitic pegmatites revised. Can. Mineral, 43, 2005–2026.

Charoy, B., 1999. Beryllium speciation in evolved granitic magmas: phosphates versus silicates. Eur, J. Mineral. 11, 135–148.

Charoy, B., Noronha, F., Lima, A., 2001. Spodumene-petalite-eucryptite mutual relationships and pattern of alteration in Li-rich aplite-pegmatite dikes from northern Portugal. Can. Mineral. 39, 729–746.

Dill, H.G., Weber, B., Gerdes, A., Melcher, F., 2008. The Fe-Mn phosphate aplite ‘Silbergrube’ near Waidhaus, Germany: epithermal phosphate mineralization in the Hagendorf-Pleystein pegmatite province. Mineral. Mag. 72(5), 1119–1144.

Elliott, T., Jeffcoate, A., Bouman, C., 2004. The terrestrial Li isotope cycle: light-weight constraints on mantle convection. Earth Planet Sci. Lett. 220, 231–245.

Elliott, T., Thomas, A., Jeffcoate, A., Niu, Y., 2006. Lithium isotope evidence for subduction-enriched mantle in the source of midocean-ridge basalts. Nature 443, 565–568.

Fransolet, A.M., 2007. Phosphate associations in the granitic pegmatites: the relevant significance of these accessory minerals. Granitic Pegmatites: The State of the Art - International Symposium. 06th – 12th May 2007, Porto, Portugal.

671 Fransolet, A.M., Keller, P., Fontan, F., 1986. The phosphate mineral associations of the
672 Tsaobismund pegmatite, Namibia. Contrib. Minera. Petrol. 92, 502–517.
673 Galliski, M.Á., Černý, P., Márquez-Zavalía, M.F., Chapman, R., 2012. An association of
674 secondary Al-Li-Be-Ca-Sr phosphates in the San Elías pegmatite, San Luis, Argentina. Can.
675 Mineral. 50, 933–942.
676 Ginsburg, A.I., 1960. Specific geochemical features of the pegmatitic process. Proc 21st Int Geol
677 Congress (Norden) 17, 111–121.
678 Grosjean, C., Miranda, P.H., Perrin, M., Poggi, P., 2012. Assessment of world lithium resources
679 and consequences of their geographic distribution on the expected development of the electric
680 vehicle industry. Renew Sustain Energy Rev. 16, 1735–1744.
681 Halama, R., Savov, I.P., Rudnick, R.L., McDonough, W.F., 2009. Insights into Li and Li isotope
682 cycling and sub-arc metasomatism from veined mantle xenoliths, Kamchatka. Contrib.
683 Mineral. Petrol. 158, 197–222, DOI 10.1007/s00410-009-0378-5.
684 Hatert, F., Ottolini, L., Schmid-Beurmann, P., 2011. Experimental investigation of the alluauditet
685 triphylite assemblage, and development of the Na-in-triphylite geothermometer: applications
686 to natural pegmatite phosphates. Contrib. Mineral. Petrol. 161, 531–546.
687 Kister, P., Laverret, E., Quirt, D., Cuney, M., Patrier Mas, P., Beaufort, D., Bruneton, P., 2006.
688 Mineralogy and geochemistry of the host-rock alterations associated with the Shea Creek
689 unconformity-type uranium deposits (Athabasca Basin, Saskatchewan, Canada). Part 2.
690 Regional-scale spatial distribution of the Athabasca Group sandstone matrix minerals. Clay
691 Clay Min. 54(3), 295–313.
692 Li, Z.X., Li, X.H., Wartho, J.A., Clark, C., Li, W.X., Zhang, C.L., Bao, C.M., 2010. Magmatic and
693 metamorphic events during the early Paleozoic Wuyi-Yunkai orogeny, southeastern south
694 China: new age constraints and pressure-temperature conditions. Geol. Soc. Am. Bull. 122,
695 772–793.
696 Linnen, R.L., Van Lichtervelde, M., Černý, P., 2012. Granitic pegmatites as sources of strategic
697 metals. Elements 8, 275–280.
698 London, D., Burt, D.M., 1982. Alteration of spodumene and lithiophilite in pegmatites of the
699 White Picacho district, Arizona. Am. Mineral. 67, 97–113.

Magma, T., Novák, M., Cempírik, J., Janoušek, V., Ullmann, C.V. and Wiechert, U. 2016. Crystallographic control on lithium isotope fractionation in Archean to Cenozoic lithium-cesium-tantalum pegmatites. Geology 44, 655-658.

Montel, J.M., 1986. Experimental determination of the solubility of Ce-monazite in SiO_2-Al_2O_3-K_2O-Na_2O melts at 800°C, 2 kbar, under H_2O-saturated conditions. Geol. 14, 659–662.

Moore, P.B., 1973. Pegmatite phosphates: descriptive mineralogy and crystal chemistry. Mineral. Rec. 4, 103–130.

Nizamoff, J., 2006. The mineralogy, geochemistry and phosphate paragenesis of the Palermo #2 Pegmatite, North Groton, New Hampshire. University of New Orleans, Unpublished Master Thesis.

Pogge von Strandmann, P.A.E., Henderson, G.M., 2015. The Li isotope response to mountain uplift. Geol. 43(1), 67–70.

Putnis, A., Austrheim, H., 2010. Fluid-induced processes: metasomatism and metamorphism. Geofluids. 10, 254–269.

Rao, C., Hatert, F., Wang, R.C., Gu, X.P., Dal Bo, F., Dong, C.W., 2015. Minjiangite, $BaBe_2(PO_4)_2$, a new mineral from Nanping No. 31 pegmatite, Fujian Province, southeastern China. Mineral. Mag. 79(5), 1195–1202.

Rao, C., Wang, R.C., Hatert, F., Baijot, M., 2014a. Hydrothermal transformations of triphylite from the Nanping No. 31 pegmatite dyke, southeastern China, Eur. J. Mineral. 26, 179–188.

Rao, C,, Wang, R.C., Hatert, F., Gu, X.P., Ottolini, L., Hu, H., Dong, C.W., Dal Bo, F., Baijot, M., 2014b. Strontiohurlbutite, $SrBe_2(PO_4)_2$, a new mineral from Nanping No. 31 pegmatite, Fujian Province, Southeastern China. Am. Mineral. 99, 494–499.

Rao, C., Wang, R.C., Hu, H., 2011. Paragenetic assemblages of beryllium silicates and phosphates from the Nanping no. 31 granitic pegmatite dyke, Fujian province, southeastern china. Can. Mineral. 49, 1175–1187.

Rao, C., Wang, R.C., Hu, H., Zhang, W.L., 2009. Complex internal texture in oxide minerals from the Nanping No. 31 dyke of granitic pegmatite, Fujian Province, southeastern China. Can. Mineral. 47, 1195–1212.

729 Rao, C., Wang, R.C., Zhang, A.C., Hu, H., 2012. The corundum + tourmaline nodules related to
730 hydrothermal alteration of spodumene in the Nanping No. 31 pegmatite dyke, Fujian
731 province, southeastern China. Can. Mineral. 50, 1623–1635.
732 Roda-Robles, E., Galliski, M.A., Roquet, M.B., Hatert, F., Paeseval, P.D., 2012. Phosphate
733 nodules containing two distinct assemblages in the Cema Granitic Pegmatite, San Luis
734 Province, Argentina: Paragenesis, composition and significance. Can. Mineral. 50(4),
735 913–931.
736 Roda-Robles, E., Pesquera, A., Fontan, F., Keller, P., 2004. Phosphate mineral associations in the
737 Cañada pegmatite (Salamanca, Spain): paragenetic relationships, chemical compositions, and
738 implications for pegmatite evolution. Am. Mineral. 89, 110–125.
739 Roda-Robles, E., Vieira, R., Pesquera, A., Lima, A., 2010. Chemical variations and significance of
740 phosphates from the Fregeneda-Almendra pegmatite field, Central Iberian Zone (Spain and
741 Portugal). Miner. Petrol. 100, 23–34.
742 Salvi, S., Pokrovski, G.S., Schott, J., 1998. Experimental investigation of aluminium-silica
743 aqueous complexing at 300°C. Chem. Geol. 151, 51–67.
744 Shigley, J.E., Brown Jr, G.E., 1985. Occurrence and alteration of phosphate minerals at the Stewart
745 pegmatite, Pala district, San Diego Co., California. Am. Mineral. 70, 395–408.
746 Shirose, Y., Uehara, S., 2014. Secondary phosphates in montebrasite and amblygonite from
747 Nagatare, Fukuoka Prefecture, Japan. J Mineral. Petrol. Sci. 109(2). 103–108.
748 Shpanov, E.P., Sidorenko, G.A., Stolyarova, T.I., 1970. Akdalaite, a new hydrous modification of
749 alumina. Zap Vses Mineral Obshch 99, 333–339 (in Russian).
750 Tang, Y., Zhao, J.Y., Zhang, H., Cai, D.W., Lv, Z.H., Liu, Y.L., Zhang, X., 2017. Precise
751 columbite-(Fe) and zircon U-Pb dating of the Nanping No. 31 pegmatite vein in northeastern
752 Cathaysia Block, SE China. Ore Geol. Rev. 83, 300-311.
753 Vignola, P., Diella, V., Oppizzi, P., Tiepolo, M., Weiss, S., 2008. Phosphate assemblages from the
754 Brissago granitic pegmatite, Western Southern Alps, Switzerland. Can. Mineral. 46, 635–650.
755 Wang, W.Y., Yang, Y.Q., Chen, C.H., Zhu, J.H., 1999. Study on the Nb and Ta-minerals from the
756 granitic pegmatites in Nanping, Fujian Province. Geol. Fujian 3, 113–134 (in Chinese with
757 English abstr.).

Wang, Y.J., Zhang, A.M., Fan, W.M., Zhao, G.C., Zhang, G.W., Zhang, Y.Z., Zhang, F.F., Li, S.Z., 2011. Kwangsian crustal anatexis within the eastern South China Block: Geochemical, zircon U-Pb geochronological and Hf isotopic fingerprints from the gneissoid granites of Wugong and Wuyi-Yunkai Domains. Lithos 127, 239–260.

Wolf, B., London, D., 1995. Incongruent dissolution of REE- and Sr-rich apatite in peraluminous granitic liquids: differential apatite, monazite, and xenotime solubilities during anatexis. Am. Mineral. 80, 765–775.

Yang, Y.Q., Wang, W.Y., Chen, C.H., Zhu, J.H., 2006. Study on the cassiterite from the Granitic pegmatites in Nanping, Fujian Province. Geol. Fujian. 25(2), 75–81.

Yang, Y.Q., Ni, Y.X., Guo, Y.Q., Qiu, N.M., Chen, C.H., Cai, C.F., Zhang, Y.P., Liu, J.B., Chen, Y.X., 1987. Rock-forming characteristics of the Xikeng granitic pegmatites in Fujian Province. Mineral. Deposits. 6, 10–21 (in Chinese with English abstract).

Yang, Y.Q., Ni, Y.X., Wang, L.B., Wang, W.Y., Zhang, Y.P., Chen, C.H., 1988. Nanpingite, a new cesium mineral. Acta Petrol Mineral Sinica. 7(1), 49–58 (in Chinese with English abstr.).

Yang, Y.Q., Wang, W.Y., Lin, G.X., Zhu, J.H., Chen, C.H., 2003. Study on the potash feldspars from the Granitic Pegmatites in Nanping, Fujian Province. Geol. Fujian. 22, 1–12 (Chinese with English abstract).

Yang, Y.Q., Wang, W.Y., Ni, Y.X., Chen, C.H., Zhu, J.H., 1994. Phosphate minerals and their geochemical evolution of granitic pegmatite in Nanping, Fujian Province. Geol. Fujian. 13, 215–226 (in Chinese with English abstract).

Yang, Y.Q., Wang, W.Y., Ni, Y.X., Chen, C.H., Zhu, J.H., 1995. A study on montebrasite in Nanping granitic pegmatite. Geol. Fujian. 14, 8–21 (in Chinese with English abstract).

Yang, Y.Q., Wang, W.Y., Ni, Y.X., Guo, Y.Q., Zhang, Y.P., Chen, C.H., 1989. Nb, Ta-minerals in Nanping pegmatites and their geological evolution. Bulletin of the Institute of Mineral Deposits, Chinese Academy of Geological Sciences. 1989(1), 55–68.

Zaraisky, G.P., Korzhinskaya, V., Kotova, N., 2010, Experimental studies of Ta_2O_5 and columbite–tantalite solubility in fluoride solutions from 300 to 550°C and 50 to 100 MPa. Mineral. Petrol. 99, 287-300.

Figure captions:

Fig. 1. Geological map showing the distribution of the Nanping pegmatite zone, the Early Paleozoic granitic and mafic plutons in the South China Block (modified after Li et al., 2010 and Wang et al., 2011).

Fig. 2. Location and simplified geological map of the Nanping pegmatite zone. (modified after Yang et al., 1987).

Fig. 3. Backscattered-electron (BSE) images of primary montebrasite and its alteration assemblages. (a) Montebrasite with fine grained muscovite and fluorapatite assemblage between quartz and albite in zone I. (b) Montebrasite with lazulite, palermoite and fluorapatite assemblage interstitial to coarse albite in zone III. Abbr.: Mtb - montebrasite, Apt - apatites, Ms - muscovite, Ab - albite, Laz-2 - secondary lazulite, Plm - palermoite.

Fig. 4. Photomicrographs and BSE images of secondary montebrasite in zone IV. (a) Primary montebrasite (Mtb) with secondary montebrasite (Mtb-1) and triphylite veinlet. (b) Secondary montebrasite (Mtb-2) replaced Fe-rich lazulite (Laz-1) among the palermoite assemblage. (c) Secondary montebrasite (Mtb-2) within the cleavages of lazulite crystals (Laz-2). (d) Secondary montebrasite (Mtb-3) among bertossaite assemblage. Abbr.: Mtb - primary montebrasite, Mtb-1, 2 and 3 - secondary montebrasite, Trp - triphylite, Laz-1,2 - secondary lazulite, Plm - palermoite, Apt - apatites, Bts - bertossaite, Ajt - arrojadite.

Fig. 5. Triangular Ca-Sr-(Mn+Fe) diagram showing the atomic proportions of compositional variations for apatite group minerals.

Fig. 6. Backscattered-electron (BSE) images of the primary montebrasite and its alteration assemblages in zone IV. (a) Montebrasite with triphylite + ludlamite + fluorapatite veins. (b) Triphylite + wagnerite + fluorapatite + fluorarrojadite assemblages along the fracture of quartz. (c) Montebrasite with wagnerite + fluorapatite assemblage. (d) Montebrasite with lazulite + palermoite + fluorapatite assemblage. (e) Montebrasite with lazulite + palermoite + muscovite

assemblage. (f) Montebrasite with simferite + fluorapatite + muscovite assemblage. Abbr.: Mtb - montebrasite, Trp - triphylite, Apt - apatites, Wag-1,2 - secondary wagnerite, Ms - muscovite, Lud - ludlamite, Ftn - tantalite-(Fe), Ajt - fluorarrojadite, Laz-2,3 - secondary lazulite, Plm - palermoite, Smf -simferite.

Fig. 7. Backscattered-electron (BSE) images of alteration assemblages of montebrasite in zone IV. (a) Palermoite + bertossaite + fluorapatite assemblage in the fracture of montebrasite. (b) Palermoite + muscovite veinlets within montebrasite. (c) Bertossaite + kulanite assemblage in the fractures of montebrasite. (d) Palermoite + bertossaite + augelite + fluorapatite assemblage nearly massive montebrasite. Abbr.: Mtb - montebrasite, Apt - apatites, Plm - palermoite, Bts - bertossaite, Kln - kulanite, Agl - augelite.

Fig. 8. Photomicrograph, BSE and SEM images of fluorapatite + akdalaite assemblages around primary montebrasite in zone IV. The photomicrograph (a) and BSE image (b) of fluorapatite + akdalaite assemblages around the primary montebrasite. (c) and (d) SEM images of fluorapatite + akdalaite assemblage, the brighter region: fluorapatite, the darker region: akdalaite. Abbr.: Mtb - primary montebrasite, Apt - apatites, Ab - albite, Akd - akdalaite, Ms - muscovite.

Fig. 9. XRD pattern of of fluorapatite + akdalaite assemblage form the Nanping No. 31 pegmatite.

Fig. 10. General hydrothermal alteration sequence of montebrasite form the Nanping No. 31 pegmatite.

Table captions:

Table 1

List of the phosphate minerals and their schematic sequence in the Nanping No. 31 pegmatite.

Table 2

The chemical composition of montebrasite in the Nanping No. 31 pegmatite.

Table 3

The chemical composition of apatite group minerals in the Nanping No. 31 pegmatite.

Table 4

The chemical composition of phosphate minerals in the Nanping No. 31 pegmatite.

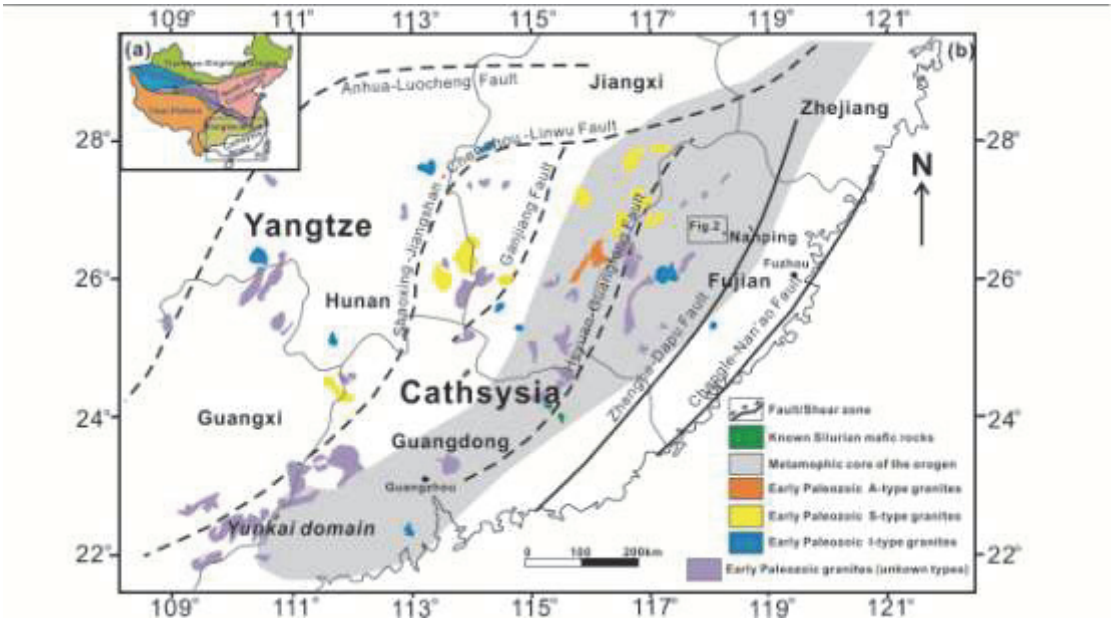
109°
111°
113°
115°
117°
119°
121°
28°
26°
24°
22°
(a)
(b)
Anhua-Luocheng Fault
Jiangxi
Zhejiang
Chaling-Yongxing-Linwu Fault
Shaoxing-Jiangshan Fault
Ganjiang Fault
Yangtze
Hunan
Fig.2
Nanping
Fuzhou
Fujian
N
Cathsysia
Guangxi
Guangdong
Guangzhou
Yunkai domain
Zhenghe-Dapu Fault
Chaozhou-Nan'ao Fault
0 100 200km
Fault/Shear zone
Known Silurian mafic rocks
Metamorphic core of the orogen
Early Paleozoic A-type granites
Early Paleozoic S-type granites
Early Paleozoic I-type granites
Early Paleozoic granites (unknown types)

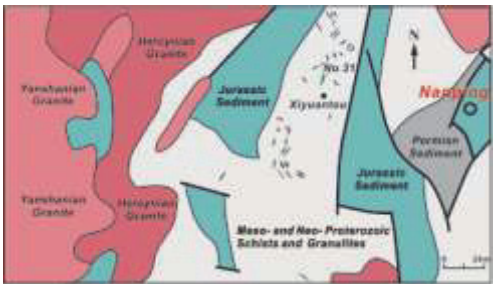
Hercynian Granite
Yanshanian Granite
Jurassic Sediment
No.31
Xiyuantou
Nanyang
Permian Sediment
Jurassic Sediment
Yanshanian Granite
Hercynian Granite
Meso- and Neo- Proterozoic Schists and Granulites

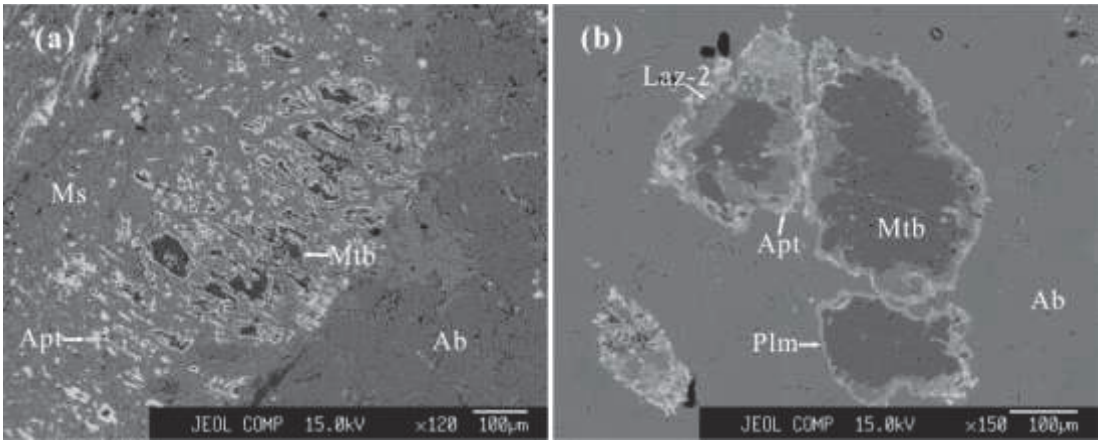
(a)
Ms
Mtb
Apt
Ab
JEOL COMP 15.0kV ×120 100μm
(b)
Laz-2
Apt
Mtb
Ab
Plm
JEOL COMP 15.0kV ×150 100μm

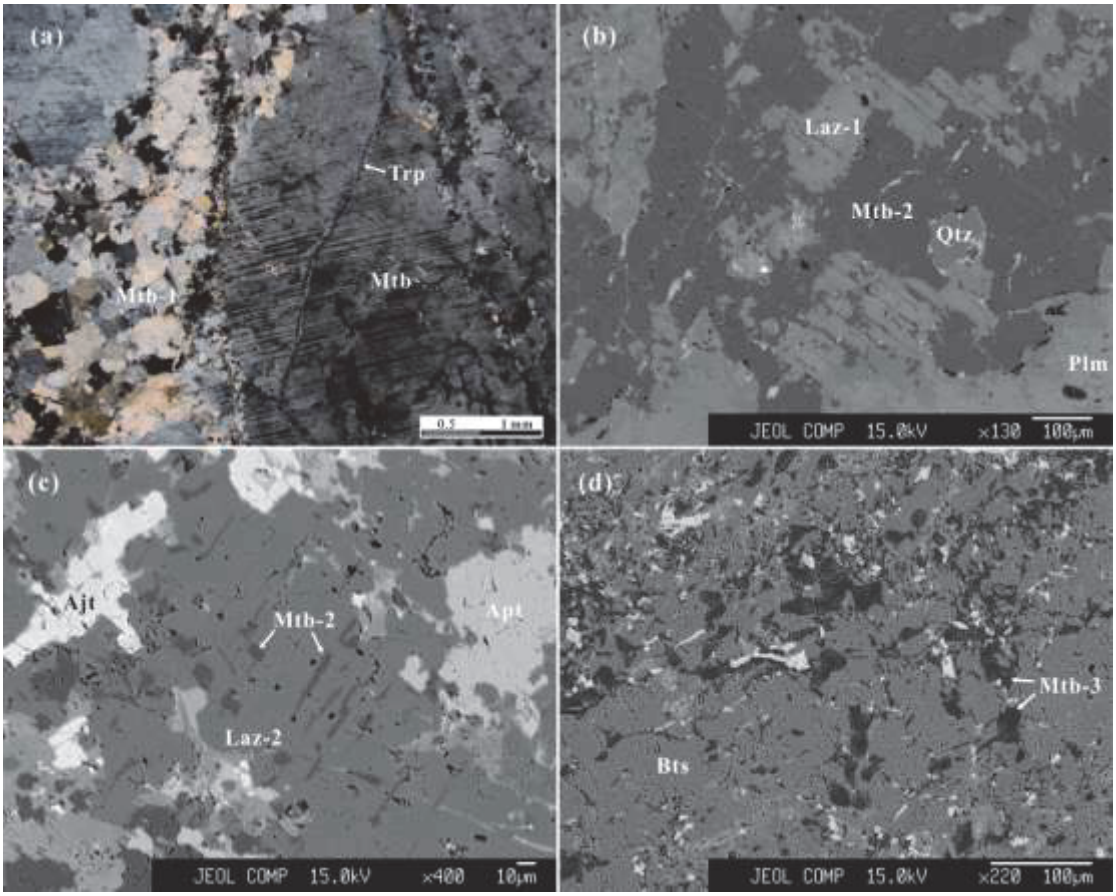
(a)
Trp
Mtb
Mtb-1
0.5 1 mm
(b)
Laz-1
Mtb-2
Qtz
Plm
JEOL COMP 15.0kV ×130 100μm
(c)
Ajt
Mtb-2
Apt
Laz-2
JEOL COMP 15.0kV ×400 10μm
(d)
Mtb-3
Bts
JEOL COMP 15.0kV ×220 100μm

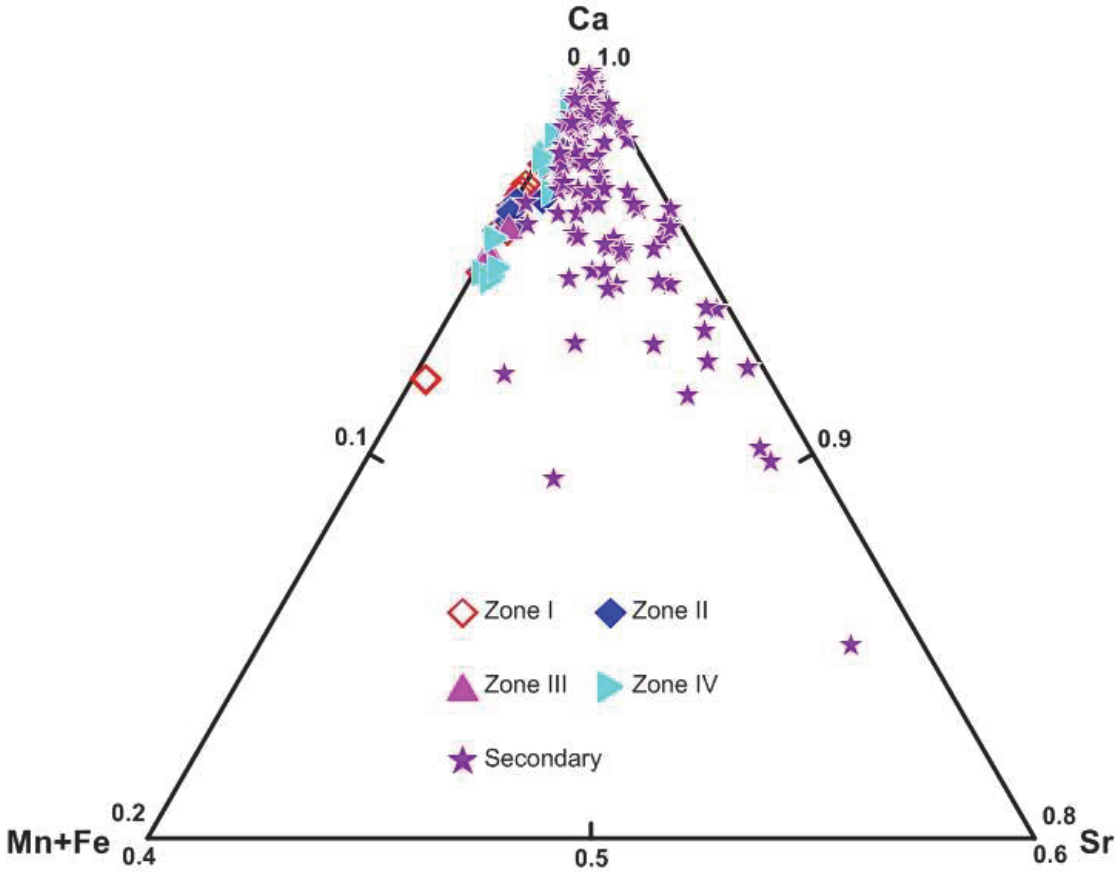
Ca
0
1.0
0.1
0.9
Zone I
Zone II
Zone III
Zone IV
Secondary
0.2
Mn+Fe
0.4
0.5
0.8
Sr
0.6

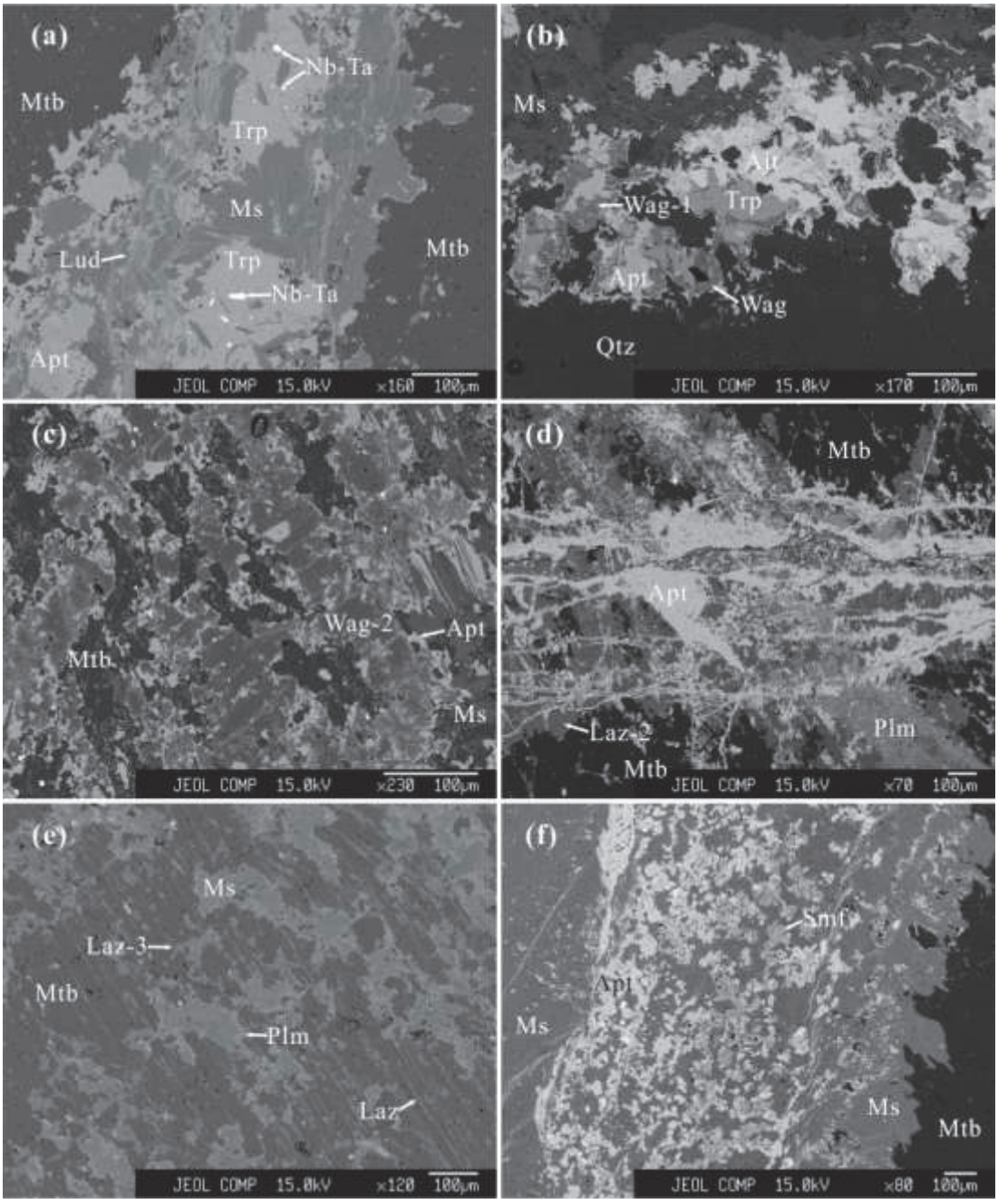
(a)
Nb-Ta
Mtb
Trp
Ms
Lud
Trp
Mtb
Nb-Ta
Apt
JEOL COMP 15.0kV ×160 100μm
(b)
Ms
Ajt
Wag-1
Trp
Apt
Wag
Qtz
JEOL COMP 15.0kV ×170 100μm
(c)
Wag-2
Apt
Mtb
Ms
JEOL COMP 15.0kV ×230 100μm
(d)
Mtb
Apt
Laz-2
Plm
Mtb
JEOL COMP 15.0kV ×70 100μm
(e)
Ms
Laz-3
Mtb
Plm
Laz
JEOL COMP 15.0kV ×120 100μm
(f)
Smf
Apt
Ms
Ms
Mtb
JEOL COMP 15.0kV ×80 100μm

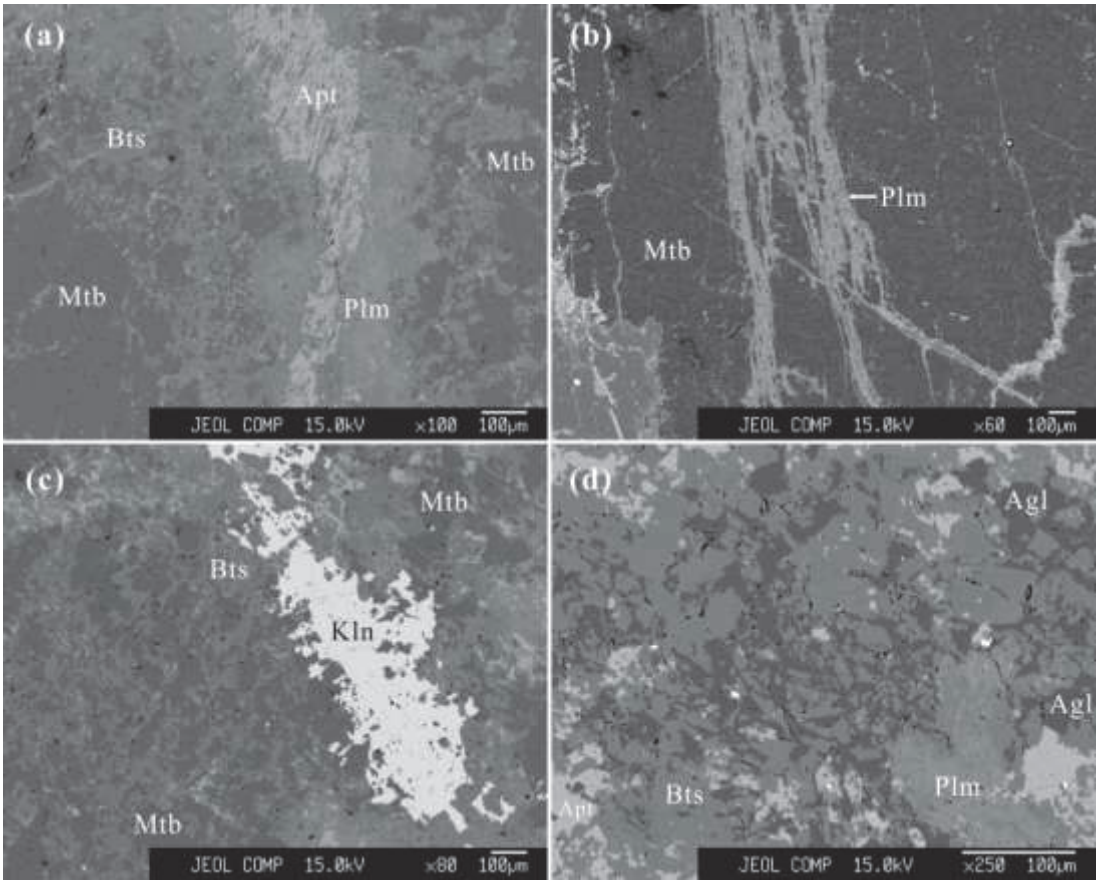
(a)
Apt
Bts
Mtb
Mtb
Plm
JEOL COMP 15.0kV ×100 100μm
(b)
Plm
Mtb
JEOL COMP 15.0kV ×60 100μm
(c)
Mtb
Bts
Kln
Mtb
JEOL COMP 15.0kV ×80 100μm
(d)
Agl
Agl
Bts
Plm
Apt
JEOL COMP 15.0kV ×250 100μm

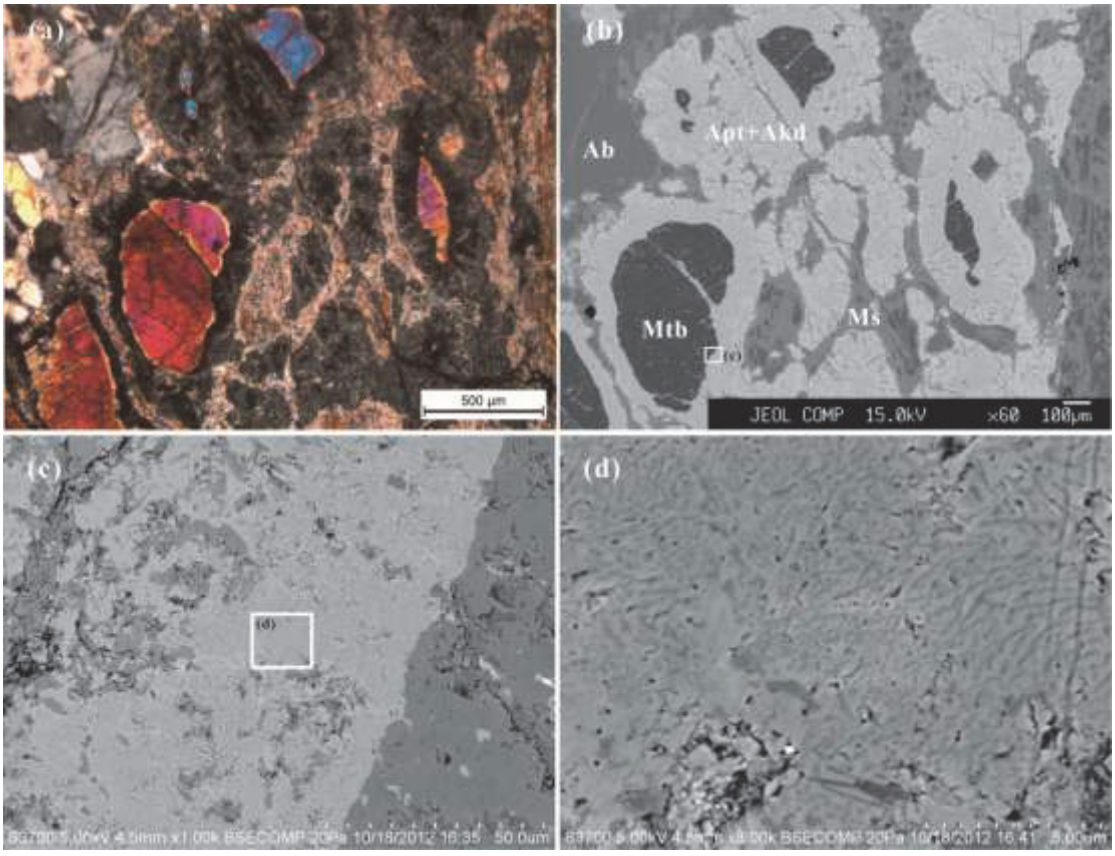
(a)
500 μm
(b)
Ab
Apt+Akd
Mtb
Ms
(c)
JEOL COMP 15.0kV ×60 100μm
(c)
(d)
(d)

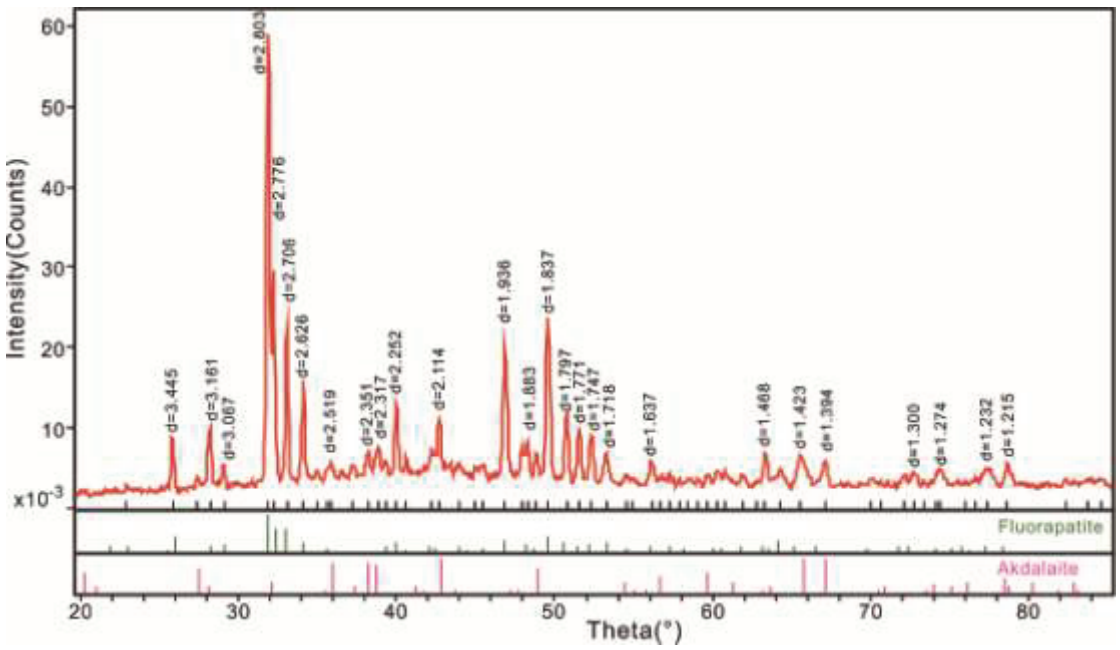
Intensity(Counts)
x10-3
60
50
40
30
20
10
d=3.445
d=3.161
d=3.067
d=2.803
d=2.776
d=2.706
d=2.626
d=2.519
d=2.351
d=2.317
d=2.252
d=2.114
d=1.936
d=1.883
d=1.837
d=1.797
d=1.771
d=1.747
d=1.718
d=1.637
d=1.468
d=1.423
d=1.394
d=1.300
d=1.274
d=1.232
d=1.215
Fluorapatite
Akdalaite
20
30
40
50
60
70
80
Theta(°)

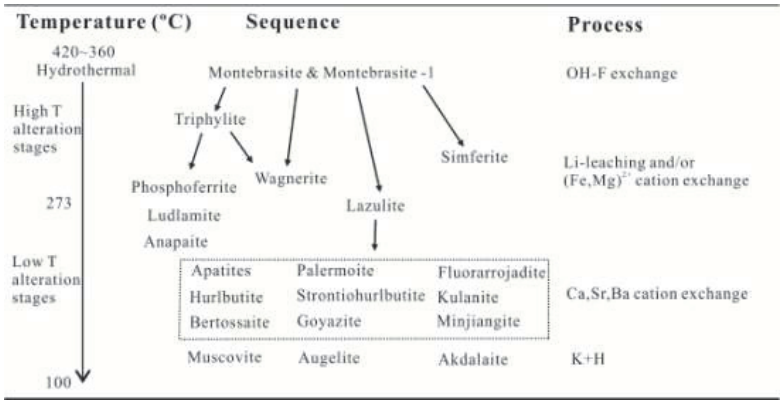
Temperature (°C)
Sequence
Process
420~360
Hydrothermal
High T
alteration
stages
273
Low T
alteration
stages
100
Montebrasite & Montebrasite -1
OH-F exchange
Triphylite
Simferite
Li-leaching and/or
(Fe,Mg)2+ cation exchange
Phosphoferrite
Wagnerite
Lazulite
Ludlamite
Anapaite
Apatites
Palermoite
Fluorarrojadite
Hurlbutite
Strontiohurlbutite
Kulanite
Ca,Sr,Ba cation exchange
Bertossaite
Goyazite
Minjiangite
Muscovite
Augelite
Akdalaite
K+H

Table 1

List of the phosphate minerals and their schematic sequence in the Nanping No. 31 pegmatite.

Mineral name	Ideal Formula	Zone					Magmatic → hydrothermal
		I	II	III	IV	V	
Monozite*	$(Ce,La,Nd,Th)PO_4$	×					
Xenotime*	$YbPO_4$	×					
Apatites	$Ca_5(PO_4)_3(F,OH)$	○	○	○	○	○	
Montebrasite	$LiAl(PO_4)(OH,F)$	×		○	√		
Triphylite	$LiFe(PO_4)$			#	#		
Lazulite	$MgAl_2(PO_4)_2(OH)_2$			×	○		
Augelite	$Al_2(PO_4)(OH)_3$			#	#		
Palermoite	$SrLi_2Al_4(PO_4)_4(OH)_4$	×		○	√	×	
Bertossaite	$CaLi_2Al_4(PO_4)_4(OH)_4$			○	√		
Goyazite	$SrAl_3(PO_4)_2(OH)_5{\cdot}(H_2O)$		×	#	#		
Crandallite	$CaAl_3(PO_4)_2(OH)_5{\cdot}(H_2O)$				×		
Kulanite	$BaFe^{2+}{}_2Al_2(PO_4)_3(OH)_3$			×	#		
Hydroxylherderite	$CaBe(PO_4)(OH)$	×	×				
Hurlbutite	$CaBe_2(PO_4)_2$	×	×		#		
Strontiohurlbutite	$SrBe_2(PO_4)_2$	×	×		#		
Minjiangite	$BaBe_2(PO_4)_2$				#		
Fluorarrojadite-(BaNa)	$BaNa_2Ca(Fe^{2+},Mn,Mg)_{13}Al(PO_4)_{11}(PO_3OH)(F,OH)_2$			#	#		
Wagnerite	$Mg_2(PO_4)F$			#	#		
Phosphoferrite	$Fe^{2+}{}_3(PO_4)_2{\cdot}3(H_2O)$				×		
Ludlamite	$Fe^{2+}{}_3(PO_4)_2{\cdot}4(H_2O)$			×	×		
Anapaite	$Ca_2Fe^{2+}(PO_4)_2{\cdot}4(H_2O)$			×	×		
Beryllonite	$NaBePO_4$	×					
Simferite	$Li(Mg,Fe^{3+},Mn^{3+})_2(PO_4)_2$				×		
Eosphorite*	$MnAl(PO_4)(OH)_2{\cdot}(H_2O)$			×			
Childrenite*	$Fe^{2+}Al(PO_4)(OH)_2{\cdot}(H_2O)$				×		
Vivianite*	$Fe^{2+}{}_3(PO_4)_2{\bullet}8(H_2O)$				×		
Ferrisichlerite*	$Li(Fe^{3+},Mn^{2+})PO_4$				×		
Vayrynenite*	$MnBe(PO_4)(OH,F)$				×		
Sicklerite*	$Li(Mn^{2+},Fe^{3+})PO_4$				×		
Autunite*	$Ca(UO_2)_2(PO_4)_2{\cdot}2\text{-}6(H_2O)$				×		

Note: √ = abundant, ○ = common, # = rare, × = very rare

*: not found in this study and referred to Yang et al. 1994

Table 2

The chemical composition of montebrasite in the Nanping No. 31 pegmatite.

	Primary montebrasite			Secondary montebrasite
	Zone I	Zone III	Zone IV	Zone IV
n	3	9	14	24
P_2O_5 wt. %	48.79(0.36)	48.92(0.54)	48.68(0.46)	48.82(0.55)
SiO_2	0.03(0.03)	0.03(0.02)	0.03(0.03)	0.05(0.09)
Al_2O_3	34.24(0.29)	34.14(0.37)	34.37(0.39)	34.27(0.48)
FeO	0.02(0.02)	0.04(0.05)	0.04(0.05)	0.09(0.10)
MnO	0.02(0.02)	0.01(0.02)	0.01(0.02)	0.01(0.02)
MgO	0.00(0.00)	0.01(0.01)	0.00(0.00)	0.07(0.14)
TiO_2	0.17(0.05)	0.07(0.06)	0.13(0.10)	0.04(0.04)
CaO	0.01(0.01)	0.02(0.02)	0.03(0.02)	0.04(0.07)
SrO	0.00(0.01)	0.01(0.01)	0.01(0.02)	0.01(0.01)
BaO	0.08(0.08)	0.05(0.06)	0.05(0.08)	0.05(0.07)
Na_2O	0.02(0.01)	0.01 (0.01)	0.01 (0.01)	0.01(0.02)
K_2O	0.01(0.01)	0.01(0.01)	0.01(0.02)	0.01(0.01)
F	1.59(1.33)	1.57(0.63)	1.27(0.78)	0.10(0.18)
Li_2O	10.26(0.08)	10.30(0.11)	10.24(0.09)	10.28(0.12)
H_2O	6.04(0.68)	6.07(0.32)	6.20(0.42)	6.83(0.14)
O=2F	-0.67(0.56)	-0.66(0.26)	-0.53(0.33)	-0.04(0.08)
Total	100.62(0.71)	100.59(0.71)	100.54(0.83)	100.63(1.07)
	Cations per formula unit: P + Si = 1			
P *apfu*	0.999	0.999	0.999	0.999
Si	0.001	0.001	0.001	0.001
Al	0.976	0.971	0.982	0.976
Fe	0.000	0.001	0.001	0.002
Mn	0.000	0.000	0.000	0.000
Mg	0.000	0.000	0.000	0.003
Ti	0.000	0.001	0.001	0.001
Ca	0.003	0.001	0.002	0.001
Sr	0.000	0.000	0.000	0.000
Ba	0.001	0.000	0.000	0.000
Na	0.001	0.000	0.000	0.000
K	0.000	0.000	0.000	0.000
Li	0.998	0.999	0.999	0.999
F	0.122	0.119	0.097	0.008
OH	0.878	0.881	0.903	0.992

FeO as the total Fe; n: the number of analyses; standard deviation in parentheses.

Table 3

The chemical composition of apatite group minerals in the Nanping No. 31 pegmatite.

	Primary apatites				Secondary apatites			
	zone I	zone II	zone III	zone IV				
n	11	7	3	16				
P_2O_5	41.69	41.56	41.61	41.66	41.05	39.30	41.00	41.38
SiO_2	0.01	-	0.01	0.02	0.86	0.01	0.06	-
CaO	53.05	54.18	53.90	53.82	54.62	52.38	52.17	50.77
FeO	0.26	0.26	0.25	0.31	0.23	0.23	0.34	-
MnO	2.74	2.20	2.46	1.65	0.47	0.47	0.97	0.56
MgO	0.01	-	0.01	0.01	0.02	-	0.02	0.01
TiO_2	0.00	0.00	-	0.01	-	0.03	-	0.01
SrO	0.12	0.10	0.26	0.24	0.59	4.62	2.72	5.93
BaO	0.05	0.06	0.05	0.02	0.05	-	-	-
Al_2O_3	0.02	0.01	0.01	0.04	0.72	0.01	0.03	0.01
Na_2O	0.07	0.01	0.01	0.01	-	0.03	-	0.02
K_2O	0.03	-	0.01	0.02	0.10	0.01	0.15	-
F	3.83	3.97	3.66	3.66	1.49	2.56	3.04	3.71
H_2O	0.09	0.06	0.05	0.18	1.19	0.50	0.33	0.00
O=2F	-1.61	-1.67	-1.54	-1.54	-0.63	-1.08	-1.28	-1.56
Total	100.35	100.75	100.76	100.10	100.76	99.06	99.56	100.84
	Cations per formula unit: P + Si = 3							
P	2.999	3.000	2.999	2.998	2.928	3.000	2.994	3.000
Si	0.001		0.001	0.002	0.072	0.000	0.006	
Ca	4.769	4.886	4.854	4.840	4.868	4.995	4.761	4.599
Fe	0.018	0.019	0.018	0.022	0.016	0.017	0.025	
Mn	0.197	0.159	0.177	0.119	0.034	0.036	0.071	0.040
Mg	0.001	0.000	0.001	0.001	0.002		0.002	0.001
Ti	0.004	0.001		0.001		0.002		0.001
Sr	0.006	0.005	0.013	0.012	0.029	0.242	0.136	0.294
Ba	0.002	0.002	0.002	0.001	0.002			
Al	0.002	0.001	0.001	0.004	0.072	0.001	0.003	0.001
Na	0.011	0.002	0.001	0.002		0.005		0.003
K	0.003	0.000	0.001	0.002	0.012	0.001	0.019	
F	1.030	1.071	0.985	0.984	0.397	0.730	0.828	1.005
OH			0.048	0.179	0.603	0.270	0.172	

FeO as the total Fe; –: below the detection limits.

Table 4

The chemical composition of phosphate minerals in the Nanping No. 31 pegmatite.

	Laz-1	Laz-2	Laz-3	Plm	Bts	Bts	Kul	Wag-1	Wag-2	Goy
n	2	22	5	Rep	Rep	Rep	3	10	8	15
P_2O_5	42.89	44.38	44.54	43.13	44.46	44.65	34.41	39.24	41.16	30.92
SiO_2	0.02	0.14	0.05	0.36	0.45	0.35	1.08	0.09	0.04	0.22
CaO	0.02	0.03	0.02	0.66	8.65	4.79	1.75	0.16	0.13	1.66
FeO	11.09	4.06	3.97	0.23	0.77	0.57	9.48	11.24	5.61	0.08
MnO	0.07	0.04	0.02	0.16	0.14	0.19	5.72	4.20	0.79	0.04
MgO	6.98	10.94	11.05	0.02	0.17	0.21	0.85	37.74	45.29	0.02
TiO_2	0.11	0.06	0.04	0.03	0.07	0.14	0.85	0.05	0.04	0.11
SrO	-	0.01	-	13.01	0.45	6.43	0.12	0.01	0.01	16.92
BaO	0.02	0.08	0.11	0.09		0.29	24.54	0.02	0.04	1.44
Al_2O_3	31.58	33.35	33.39	31.00	32.04	31.27	16.26	0.05	0.04	33.50
Na_2O	-	0.01	-	0.02	0.03	0.06	0.11	0.01	-	0.04
K_2O	-	0.05	0.01	0.00	0.00	0.00	0.22	0.01	0.01	0.04
F	-	-	-	0.25	1.38	1.73	0.01	11.08	7.77	0.85
H_2O	6.05	6.28	6.28	6.01	5.61	5.44	5.02	-0.29	1.72	14.93
Li_2O				4.57	4.72	4.71				
O=2F				-0.10	-0.58	-0.73	0.00	-4.65	-3.26	-0.36
Total	98.83	99.44	99.48	99.43	98.37	100.09	100.42	98.95	99.39	100.41
P	1.999	1.992	1.997	3.961	3.953	3.964	2.903	0.997	0.999	1.983
Si	0.001	0.008	0.003	0.039	0.047	0.036	0.097	0.003	0.001	0.017
Ca	0.001	0.002	0.001	0.076	0.961	0.531	0.167	0.005	0.004	0.133
Fe	0.511	0.180	0.176	0.021	0.068	0.050	0.821	0.282	0.135	0.005
Mn	0.003	0.002	0.001	0.014	0.012	0.016	0.504	0.107	0.019	0.002
Mg	0.573	0.865	0.873	0.004	0.027	0.033	0.129	1.690	1.936	0.002
Ti	0.004	0.002	0.001	0.002	0.006	0.011	0.063	0.001	0.001	0.007
Sr		0.000		0.818	0.028	0.391	0.006	0.000	0.000	0.744
Ba	0.000	0.002	0.002	0.004		0.012	0.958	0.000	0.000	0.043
Al	2.049	2.084	2.085	3.963	3.966	3.864	1.916	0.002	0.001	2.992
Na		0.001		0.005	0.006	0.011	0.021	0.001		0.005
K		0.004	0.001	0.000	0.000	0.000	0.030	0.000	0.000	0.005
Li				1.995	1.994	1.988				
F				0.084	0.460	0.575	0.003	1.053	0.704	0.204
OH	2.000	2.000	2.000	3.916	3.540	3.425	2.997	0.000	0.296	6.796

FeO as the total Fe; –: below the detection limits. Structural formulas were calculated on the basis of 2, 4, 3, 1, 2and 2 (P+Si) atoms for lazulite, palermoite-bertossaite, kulanite, wagnerite and goyazite, respectively. Abbr.: Laz - lazulite, Plm - palermoite, Bts - bertossaite, Kul - kulanite, Wag - wagnerite, Goy - goyazite.

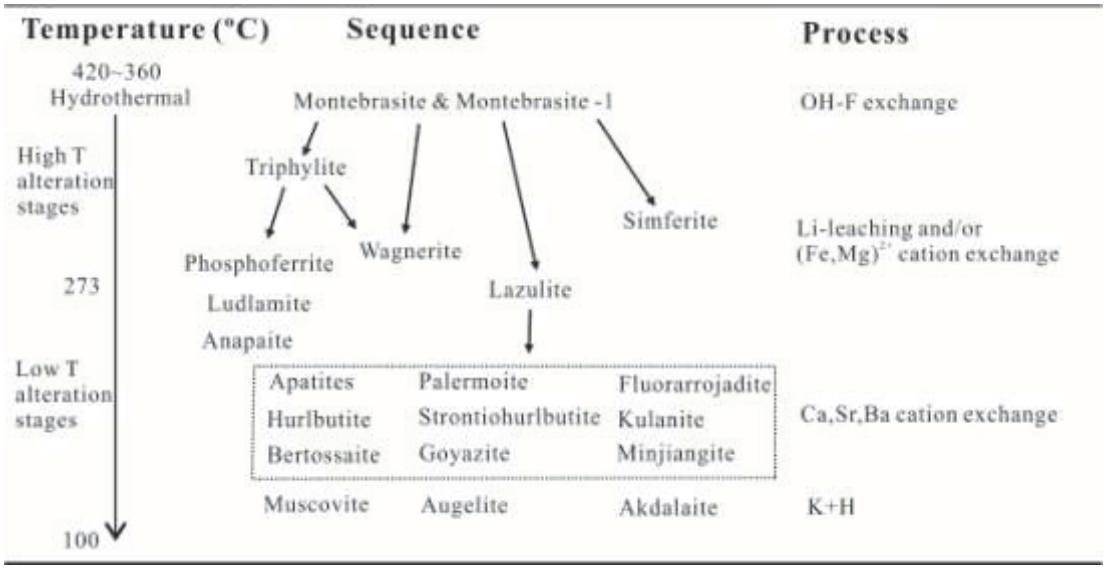
Temperature (°C)
Sequence
Process
420~360
Hydrothermal
Montebrasite & Montebrasite -1
OH-F exchange
High T
alteration
stages
Triphylite
Simferite
Li-leaching and/or
(Fe,Mg)2+ cation exchange
Phosphoferrite
Wagnerite
273
Ludlamite
Lazulite
Anapaite
Low T
alteration
stages
Apatites
Palermoite
Fluorarrojadite
Hurlbutite
Strontiohurlbutite
Kulanite
Ca,Sr,Ba cation exchange
Bertossaite
Goyazite
Minjiangite
Muscovite
Augelite
Akdalaite
K+H
100